

AD-A074 951

DREXEL UNIV PHILADELPHIA PA DEPT OF PHYSICS AND ATMOS--ETC F/G 7/4
STUDY OF TWO-PHOTON ABSORPTION AND AMPLIFICATION PROCESSES IN G--ETC(U)
SEP 79 L M NARDUCCI

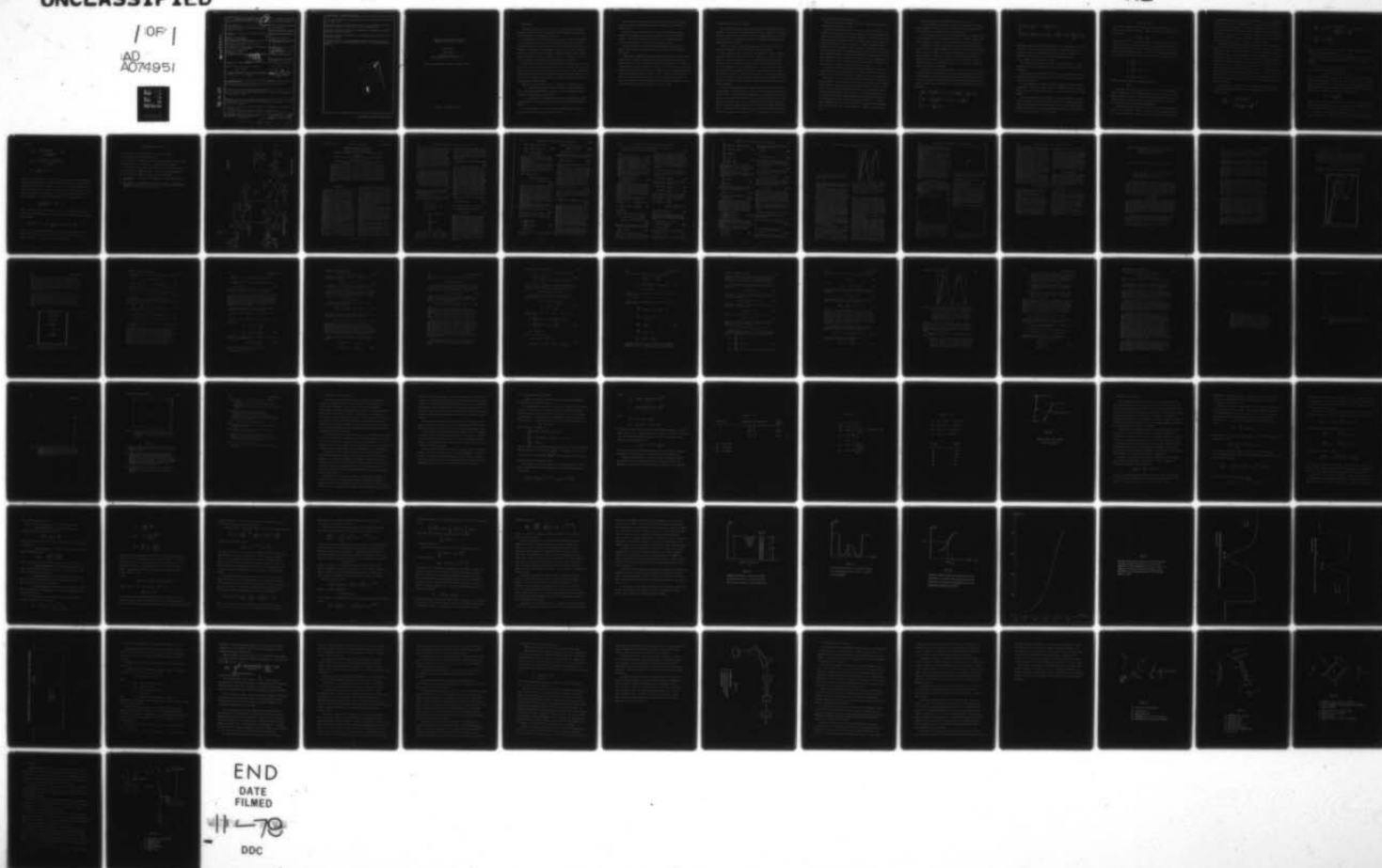
DAAG29-78-G-0098

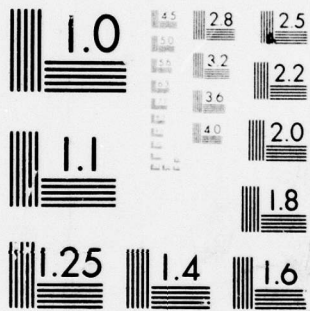
NL

UNCLASSIFIED

/ OF /

AD
A074951





AD A 074951

DDC FILE COPY

SECURITY CLASSIFICATION OF THIS PAGE (When Data Entered)

REPORT DOCUMENTATION PAGE		READ INSTRUCTIONS BEFORE COMPLETING FORM
1. REPORT NUMBER	2. GOVT ACCESSION NO.	3. RECIPIENT'S CATALOG NUMBER
4. TITLE (and Subtitle) Study of Two-Photon Absorption and Amplification Processes in Gases.		5. TYPE OF REPORT & PERIOD COVERED 8/1/76-6/30/79
7. AUTHOR(s) Lorenzo M. Narducci / Ph.D.		6. PERFORMING ORG. REPORT NUMBER
9. PERFORMING ORGANIZATION NAME AND ADDRESS Physics Department, Drexel University, Philadelphia, PA 19104		8. CONTRACT OR GRANT NUMBER(s) DAAG29-78-G-0098
11. CONTROLLING OFFICE NAME AND ADDRESS Office of Naval Research Arlington, VA 22217		10. PROGRAM ELEMENT, PROJECT, TASK AREA & WORK UNIT NUMBERS
14. MONITORING AGENCY NAME & ADDRESS (if different from Controlling Office)		12. REPORT DATE 1 September 79
15. SECURITY CLASS. (of this report)		13. NUMBER OF PAGES 82
16. DISTRIBUTION STATEMENT (of this Report) Distribution of this report is unlimited		15a. DECLASSIFICATION/DOWNGRADING SCHEDULE
17. DISTRIBUTION STATEMENT (of the abstract entered in Block 20, if different from Report)		
18. SUPPLEMENTARY NOTES Some section of this report have been completed in collaboration with Mr. L.G. Johnson and Mr. E.J. Seibert.		
19. KEY WORDS (Continue on reverse side if necessary and identify by block number) Lasers, Nonlinear spectroscopy, quantum optics, electromagnetic propagation in active atomic systems.		
20. ABSTRACT (Continue on reverse side if necessary and identify by block number) This report summarizes our theoretical and experimental findings. It is divided into 8 sections. Section 1 contains a general description of the problem and a summary of the main results. Section 2 contains the theory of two-photon amplification. Section 3 details the requirements for the selection of an appropriate active medium.		

DD FORM 1 JAN 73 1473

EDITION OF 1 NOV 65 IS OBSOLETE
S/N 0102-014-6601

SECURITY CLASSIFICATION OF THIS PAGE (When Data Entered)

79 10 11 034

Section 4 describes the pumping requirements and the handling and preparation of the vapor cell.

Section 5 contains a description of the curve of growth method which has been used in the work to measure the density of Calcium vapor.

Section 6 describes the details of operation of the pump dye laser and of the second harmonic generation.

Section 7 contains a description of the construction and operation of the infrared dye laser.

Section 8 contains a description and technical details of the timing circuitry used to fire the pump and probe lasers in a preassigned temporal sequence.

Accession For	
NTIS	General
DDC TAB	
Unannounced	
Justification	
By	
Distribution/	
Availability Codes	
Dist	Available/or special

STUDY OF TWO-PHOTON ABSORPTION AND
AMPLIFICATION PROCESSES IN GASES

A final report

submitted by

Lorenzo M. Narducci
Physics Department, Drexel University

Office of Naval Research Agreement #DAAG29-78-G-0098

August 1, 1976-June 30, 1979

1. Introduction

The original objective of this project was to demonstrate the possibility of energy extraction from an inverted atomic system through a new kind of non-linear process called two-photon amplification.

We have performed a theoretical study of the proposed effect, established a set of guidelines for the selection of a suitable atomic system and carried out the construction of the required multi-laser system. We have not been successful yet in observing two-photon amplification within the time allotted to the program mainly because of the lack of suitable tunable dye lasers. However, many of the original technical difficulties have been solved, and activities are still in progress along the originally proposed lines of research.

Several unsatisfactory features of the commercial units which were purchased for our work have been corrected (temperature control of the dye and circulating water lines, jitter in the initiation of laser output, etc.). Other improvements and modifications required for the simultaneous operation of the multi-laser system are presently under way in an attempt to complete the experimental phase of this project to our satisfaction.

Among the main advances that have been carried out, we should mention:

i) the design of a Ruby laser-pumped high power infrared tunable dye laser operating around 9153 \AA with a considerably broader tuning range than originally anticipated from published data.

ii) construction of a tunable ultraviolet source consisting of a flash lamp pumped dye laser and angle-tuned second harmonic crystal for operation at 2721 \AA .

iii) establishment of a set of procedures for handling, testing and monitoring the active atomic system (Calcium vapor).

iv) the design of a vacuum system for the preparation of the vapor sample and for the mixing of an appropriate amount of buffer gas. The latter was chosen to be Xe.

v) the design and construction of an accurate timing system capable of driving the ultraviolet and infrared laser pulses in a prescribed temporal sequence. The timing requirements have been solved after rebuilding the spark-gap circuit in one of our flash lamp-pumped dye lasers.

Details concerning the status of our instrumentation and the prospects for the observation of the proposed effect are described in the main text of this report.

There remains a potentially troublesome aspect of our proposed scheme which resides in the incomplete and often inaccurate knowledge of all the necessary atomic parameters. The intensity-dependent gain of the amplifier is a sensitive function of the oscillator strengths which enter in the non-linear atomic susceptibility. An uncertainty of the order of a factor of 2 or 3 could be critical for a successful implementation of our scheme. Because, however, recent interest in four-wave mixing processes has prompted renewed investigation in Calcium vapor (as well as Strontium, Barium and Magnesium) a more accurate theoretical analysis of the parameters in question is expected to be within reach.

2. Theoretical outline and background

The idea of producing two-photon stimulated emission and amplification was mentioned in early papers by Sorokin and Braslan¹ and by Prokhorov². To the best of our knowledge, the first dynamical study of two-photon amplification was carried out by Estes and Shammas jointly with this principal investigator³ using the Bloch-Maxwell formalism.

Prior to this work, coherent two-photon absorption had been studied by Belenov and Poluektov⁴ and at about the same time by Takatsuji⁵.

From a conceptual point of view, the scheme suggested by Estes, Narducci and Shammas can be described qualitatively as follows. One assumes inversion between two levels of the same parity. If no allowed radiative processes or collision induced decays exist, the natural relaxation of the excited atoms back to the ground state will be relatively long. If a strong incident field with a carrier frequency approximately equal to one-half of the atomic transition frequency is allowed to interact with the atoms, a non-linear polarization can be induced which oscillates at the same frequency as the incident wave. The atoms, then re-radiate at this frequency and, under appropriate conditions, the wave is amplified.

The details of the model are made more explicit in the enclosed reprints. Here, two facts are worth mentioning: first of all, if allowed radiative transitions from the excited state are to be eliminated, it is reasonable to give preference to atoms with an excited state that lies directly above and has the same parity as the ground state; secondly, the magnitude of the non-linear polarization is expected to be much smaller in the absence of near resonant intermediate states. The quasi-resonant enhancement, which is very convenient for observing two-photon absorption in atomic vapors, will be absent here because of the need

for a long lifetime of the upper level.

Thus, the selection of a suitable atomic species must be made with these two conflicting requirements in mind.

Our theoretical understanding of the process is rather satisfactory. The evolution of the propagating pulse through the inverted atomic medium has been described in terms of coupled field-matter equations. In the limiting case of coherent propagation (negligible effects associated with the irreversible longitudinal and transverse atomic relaxations) the pulse evolution has been described by an "area equation" similar in spirit to the equations proposed by Arecchi and Bonifacio⁶ for a one-photon amplifier, and by McCall and Hahn⁷ for self-induced transparency. Our area equation, however, describes the evolution of the total pulse energy and thus is directly related to a measurable quantity (by contrast the "area" of Arecchi-Bonifacio and McCall-Hahn is defined as the integrated pulse envelope which is not directly observable).

We have discovered frequency modulation effects which are entirely absent in the conventional single-photon amplifier. These are presently under investigation. The available results will be summarized at the end of this section.

With reference to Fig. 1 of the enclosed reprint "Theory of a two-photon laser amplifier" by L.M. Narducci, W.W. Eidson, P. Furcinitti, and D.C. Eteson⁸, we note that the assumed energy level structure of our model system has active levels of the same parity (energy separation $\hbar\omega_{ba}$). No direct dipole transition can occur between these levels; however, a non-linear polarization can be induced with the help of the dipole-allowed intermediate states which have been labelled collectively with the state vector symbol $|j\rangle$. It is assumed that a population inversion can be established between the excited and ground state and that a pulse with a carrier frequency $\omega \approx \frac{\omega_{ba}}{2}$ is incident upon the system.

The main results of the calculations reported in Ref. (9) are:

i) The evolution of the atomic system can be described by a collection of three variables; these satisfy three coupled differential equations which bear a strong formal similarity with the Bloch equations.

ii) A non-linear polarization oscillating with the same carrier frequency as the incident pulse can be induced in the medium. The atoms re-radiate and, under appropriate conditions, cause an amplification of the incident pulse.

To be precise, additional components of the non-linear polarization may also be induced and competing paths for the release of the stored atomic energy can be opened (for example, third harmonic generation can be supported in the inverted vapor). A simple way to eliminate the effects of the non-linear polarization at frequency 3ω is to prepare the incident pulse in a state of circular polarization. The atomic selection rules, in this case, prevent the generation of third harmonic light.

If one ignores the irreversible dephasing processes induced by collisions (it appears safe to ignore the relaxation of the population inversion because of the long lifetime of the excited state and the low pressure at which the system is expected to operate), the coupled equations describing the evolution of the atomic variables and the propagation of the field intensity and phase have been shown to be

$$\begin{cases} \dot{R}_1 = \left[\frac{k_{bb} - k_{aa}}{4\hbar} \mathcal{E}_0^2 + (2\omega - \omega_{ba} + 2 \frac{\partial \psi}{\partial t}) \right] R_2 + \frac{k_{ab}}{2\hbar} \mathcal{E}_0^2 R_3 \\ \dot{R}_2 = - \left[\frac{k_{bb} - k_{aa}}{4\hbar} \mathcal{E}_0^2 + (2\omega - \omega_{ba} + 2 \frac{\partial \psi}{\partial t}) \right] R_1 \\ \dot{R}_3 = - \frac{k_{ab}}{2\hbar} \mathcal{E}_0^2 R_1 \end{cases}$$

$$\left\{ \begin{array}{l} \left(c \frac{\partial}{\partial x} + \frac{\partial}{\partial t} \right) \mathcal{E}_0^2 = \frac{\omega N k_{ab}}{\epsilon_0} R_1 \mathcal{E}_0^2 \\ \left(c \frac{\partial}{\partial x} + \frac{\partial}{\partial t} \right) (2\omega - \omega_{ba} + 2 \frac{\partial \psi}{\partial t}) = \frac{\omega N k_{ab}}{\epsilon_0} \left(\dot{R}_2 - \frac{k_{tb} - k_{aa}}{2k_{ab}} \dot{R}_3 \right) \end{array} \right.$$

The atomic variables R_1 and R_2 are proportional to the out-of-phase and in-phase components of the non-linear polarization; R_3 is the population difference between the excited and ground states of the system; \mathcal{E}_0^2 is proportional to the slowly varying intensity envelope of the propagating pulse and $2\omega - \omega_{ba} + 2 \frac{\partial \psi}{\partial t}$ is the instantaneous detuning.

It is obvious, by inspection, that the atomic equations bear a striking resemblance to the standard Bloch equations for two-level atoms with two main differences:

a) the role of the conventional Rabi frequency (essentially the envelope of the driving field in the ordinary two-level Bloch formalism) is played by the field intensity \mathcal{E}_0^2 .

b) the detuning term contains an intensity-dependent contribution which is immediately suggestive of the existence of chirping and frequency modulation effects even if the resonance condition $2\omega - \omega_{ba} = 0$ is met at the input of the amplifier.

The field equations for the intensity \mathcal{E}_0^2 and the detuning also resemble the field equations for two-level systems. Here, however, the driving polarization is directly proportional to the field envelope itself. Under coherent propagation conditions (i.e. on neglecting irreversible atomic decay processes) the atomic variables satisfy the conservation law

$$R_1^2 + R_2^2 + R_3^2 = 1$$

just as the corresponding Bloch variables for two-level systems do. If, in addition, the resonance condition $\omega = \frac{\omega_b a}{2}$ is satisfied, the additional conservation law

$$R_2 - \gamma R_3 = R_2(0) - \gamma R_3(0) = -\gamma$$

is satisfied, where γ is the ratio of certain electric susceptibility coefficients (see eqs. (2.7) and (5.4) of Ref. (9)). Because of these relations between the three Bloch variables, the resonance propagation is governed by only one independent atomic parameter. This has been demonstrated explicitly by showing the validity of the exact formal solution of the Bloch equations

$$\begin{aligned} R_1 &= \frac{R_3^e}{\sqrt{1+\gamma^2}} \sin \sigma \\ R_2 &= \frac{R_3^e \gamma}{1+\gamma^2} (\cos \sigma - 1) \\ R_3 &= \frac{R_3^e}{1+\gamma^2} (\cos \sigma + \gamma^2) \end{aligned}$$

where R_3^e is the initial equilibrium population and

$$\frac{\partial \sigma}{\partial \tau} = \omega_R$$

The result is all the more remarkable if we observe that the parameter σ which is proportional to the accumulated energy of the pulse from the leading edge ($\tau = 0$) to a given time τ , satisfies an "area equation" which can be integrated exactly to yield exact analytic predictions on the behavior of the total pulse energy for sufficiently long amplifiers.

We refer to the enclosed reprints for details concerning the quantitative predictions of this theory. Here it is worth mentioning that numerical solutions of the coupled Maxwell-Bloch equations have confirmed the above features

of the propagation problem and have shown in addition that, above threshold for amplification, no intrinsic limitations to the traveling pulse peak power is imposed by the non-linear process. Of course, in actual practice, it is expected that additional nonlinearities will become important as the peak power of the incident pulse becomes larger and larger. Nonetheless, it is rather remarkable that the usual power saturation effects, which are well known in ordinary laser amplifiers, are absent in a two-photon amplifying medium.

Under ordinary experimental conditions with vapor pressure of the order of 10^{-3} - 10^{-1} torr and buffer gas pressure in the range 10-100 torr, the irreversible decay processes induced by collisions and the loss of atomic coherence are no longer negligible. We have generalized the Bloch equations in the traditional way with the addition of phenomenological decay terms for the components R_1 , R_2 of the Bloch vector and analyzed the evolution of pulses of various widths by numerical techniques. Solutions have been obtained over the entire range of interest from the coherent limit (pulse duration much shorter than the atomic decay time T_2) to the rate equation limit (pulse duration much larger than T_2). As in the case of an ordinary laser amplifier, the main signature of the loss of the atomic coherence is the reduction and eventual disappearance of the pulse envelope modulation.

In the extreme rate equation limit, the polarization variables R_1 and R_2 can be eliminated adiabatically and the pulse evolution is governed by the coupled equations

$$\frac{\partial R_3}{\partial \tau} = - \frac{T_2 \left(\omega_R / \sqrt{1+y^2} \right)^2}{1 + \left[T_2 \left(\frac{y}{\sqrt{1+y^2}} \omega_R + \Omega \right) \right]^2} R_3$$

$$\frac{\partial \omega_R}{\partial \eta} = g T_2 \sqrt{1+\gamma^2} \frac{(\omega_R / \sqrt{1+\gamma^2})^2}{1 + \left[T_2 \left(\frac{\gamma}{\sqrt{1+\gamma^2}} \omega_R + \Omega \right) \right]^2} R_3 - l \omega_R$$

$$\frac{\partial \Omega}{\partial \eta} = -g \gamma \frac{\partial R_3}{\partial \tau}$$

where τ and η are the usual local time and scaled distance variables, and Ω denotes the instantaneous detuning $2\omega - \omega_{ba} + 2 \frac{\partial \psi}{\partial \tau}$.

The role of frequency modulation in the propagation of a pulse has been investigated only recently by our group. A few preliminary results are available:

i) in the coherent regime, the field equations for the intensity ω_R and the detuning Ω imply the conservation law

$$\omega_R(\eta, \tau) \Omega(\eta, \tau) = \omega_R(\eta=0, \tau) \delta$$

where δ is the detuning $2\omega - \omega_{ba}$ at the input of the amplifier and where the linear scattering losses have been ignored for simplicity. It is clear that, unless the incident pulse is exactly tuned for two-photon resonance ($\delta = 0$), frequency modulation will accompany the reshaping of the pulse envelope. More specifically, the instantaneous detuning is predicted to be

$$\Omega(\eta, \tau) = \delta \times \frac{\omega_R(\eta=0, \tau)}{\omega_R(\eta, \tau)}$$

where $\omega_R(\eta=0, \tau)$ is the intensity profile at the input of the amplifier. It is clear that the magnitude of the ratio $\omega_R(0, \tau)/\omega_R(\eta, \tau)$ controls the size of the instantaneous detuning relative to its input value.

ii) in the rate equation regime the polarization variables R_1 and R_2 follow the variations of the field intensity adiabatically according to the

relations

$$R_1 = \frac{T_2 \omega_R / \sqrt{1+\gamma^2}}{1 + (T_2 A)^2} R_3$$

$$R_2 = - \frac{(T_2 A) \cdot T_2 \cdot (\omega_R / \sqrt{1+\gamma^2})}{1 + (T_2 A)^2} R_3$$

$$A \equiv \frac{\gamma}{\sqrt{1+\gamma^2}} \omega_R - \Omega$$

The above equations predict a dependence of R_1 and R_2 on the intensity-dependent detuning variable A which is reminiscent of the usual dispersion relations for single photon transitions. However, in this case, R_1 and R_2 are proportional to the field intensity (rather than to the field amplitude) and furthermore, the locations of the peak of R_1 and of the zero of R_2 are intensity-dependent. One of the consequences of these dispersion relations is the conservation law

$$\frac{\partial}{\partial \eta} \left(\frac{\gamma}{\sqrt{1+\gamma^2}} \omega_R - \Omega \right) = 0$$

which relates the instantaneous field intensity ω_R and the frequency detuning Ω . Here again we find that chirping is associated with the pulse evolution according to the relation

$$\Omega(\eta, \tau) = 2\omega - \omega_{ba} + \frac{\gamma}{\sqrt{1+\gamma^2}} [\omega_R(\eta, \tau) - \omega_R(0, \tau)]$$

The behavior of Ω for the intermediate regime where the incident pulse width is comparable to the atomic transverse relaxation time T_2 is too complex to be studied analytically. A numerical analysis is in progress.

References for Section 2

1. P.P. Sorokin, N. Braslan, IBM J. Res. Dev. 8, 177 (1964).
2. A.M. Prokhorov, Science 149, 828 (1965).
3. L.E. Estes, L.M. Narducci, B. Shamma, Nuovo Cimento Lett. 1, 175 (1971).
4. E.M. Belenov, I.A. Poluektov, Sov. Phys. JETP 29, 754 (1969).
5. M. Takatsuji, Physica (Utr.) 51, 265 (1971), Phys. Rev. B2, 340 (1970).
6. F.T. Arecchi, R. Bonifacio, IEEE. J. Quant. Electr. QE-1, 169 (1965).
7. S.L. McCall, E.L. Hahn, Phys. Rev. Lett. 18, 1019 (1965).
8. L.M. Narducci, W.W. Eidson, P. Furcinitti, D.C. Eteson, Phys. Rev. A16, 1665 (1977).
9. L.M. Narducci, L.G. Johnson, E.J. Seibert, W.W. Eidson, in Coherence in Spectroscopy and Modern Physics, Eds. F.T. Arecchi, R. Bonifacio, M.O. Scully (Plenum Press, N.Y. 1978) p. 131.

Theory of a two-photon laser amplifier*

Lorenzo M. Narducci and William W. Eidson

Department of Physics and Atmospheric Science, Drexel University, Philadelphia, Pennsylvania 19104

Paul Furcinitti

Department of Biochemistry, Pennsylvania State University, University Park, Pennsylvania 16802

Donald C. Eteson

Electrical Engineering Department, Worcester Polytechnic Institute, Worcester, Massachusetts 01609

(Received 27 January 1977; revised manuscript received 16 June 1977)

We discuss the propagation of an electromagnetic pulse through an active medium prepared in a state of inversion between two levels of the same parity. Since no electric dipole transition is possible between the chosen atomic levels, we investigate the possibility of amplification of an injected signal having a carrier frequency equal to one-half the atomic-transition frequency. We show that under suitable conditions a nonlinear atomic polarization can be generated which oscillates at the same frequency as the incident electromagnetic pulse. The coupled atom-field evolution is described by the usual self-consistent approach. When atomic relaxation effects are negligible, we derive an equation describing the spatial evolution of the energy of the propagating pulse. From this equation we characterize the threshold condition for power amplification and classify the multiple steady-state solutions of the propagation problem. The evolution of the pulse envelope through the amplifier is analyzed with the help of a hybrid computer simulation. Pulse-envelope modulation and multiple-pulse formation even in the asymptotic limit of long amplifiers are displayed.

I. INTRODUCTION

The possibility of producing two-photon stimulated decay and power amplification in a pumped active medium was suggested, apparently for the first time, by Prokhorov¹ and Sorokin and Branslau.² Since then, considerable progress has been made in understanding the dynamics of coherent two-photon processes.³

Much of the recent work has focused on situations in which the atoms are initially in their ground state; the results have shown surprising qualitative similarities between coherent two-photon processes and their single-photon counterparts⁴ (the term coherent is used here, and henceforth, to characterize situations where the atomic relaxation times are much longer than the duration of the propagating pulse). Thus, self-induced transparency, pulse-amplitude and frequency modulation, adiabatic following, and coherent transfer of atomic population have been described theoretically.⁵ Experiments on coherent two-photon processes have also been reported.⁶

More limited attention has been directed to the propagation of a pulse in an inverted medium when the active levels are not coupled by a direct electric dipole transition.⁷⁻⁹ Past experience with one-photon processes has shown that rather minor formal differences exist between the working equations for an amplifying medium¹⁰ and those which are appropriate for an absorbing system.¹¹ This

is still true in the theoretical analysis of atoms undergoing two-photon emission or absorption. However, the theory of a two-photon amplifier predicts interesting effects which have no analog if the atoms are initially unexcited. Thus, for example, we find that, while a two-photon absorber allows the propagation of a Lorentzian-shaped steady-state pulse, the coherent two-photon amplifier cannot support a steady-state-pulse envelope. On the other hand, the pulse energy satisfies an equation that allows different classes of steady-state solutions.

In this paper, we discuss the theory of a degenerate two-photon amplifier. The term degenerate indicates that the carrier frequency of the incident pulse is approximately one-half of the atomic transition frequency. We require the incident pulse to satisfy the slowly varying envelope and phase approximation, and in addition we restrict our attention to pulse durations which are sufficiently smaller than the atomic incoherent relaxation times.

Our analysis evolves along the lines mapped out by Estes *et al.*⁷ We describe in some detail the derivation of the coupled atom-field equations of motion and construct an equation for the pulse energy which is reminiscent of the well known Arecchi-Bonifacio "area equation" for a one-photon amplifier. In this case, however, we discover a much richer variety of solutions that include single as well as multiple pulses. In addition, our energy

equation is integrable and leads to explicit predictions regarding the asymptotic (large-distance) behavior of the pulse energy. The threshold condition for power amplification requires simultaneously an appropriate population inversion between the active levels and a sufficiently large input energy. As a result, small-signal amplification cannot be supported by a two-photon amplifier. On the other hand, if the power amplification conditions are met, a propagating pulse undergoes envelope modulation leading to pulse sharpening and, under appropriate conditions, multiple-pulse formation.

II. BLOCH EQUATIONS FOR THE ACTIVE MEDIUM

We formulate our calculations for a typical atomic system with an energy-level diagram such as shown in Fig. 1. The levels labeled $|a\rangle$ and $|b\rangle$ are assumed to have identical parity, while the intermediate states, labeled $|j\rangle$, are coupled to either $|a\rangle$ or $|b\rangle$ (or both) by a direct dipole transition.

The total Hamiltonian of the system has the form

$$H = E_a |a\rangle\langle a| + E_b |b\rangle\langle b| + \sum_j E_j |j\rangle\langle j| - \vec{p} \cdot \vec{\mathcal{E}}(x, t), \quad (2.1)$$

where the electric field $\vec{\mathcal{E}}(x, t)$ has the familiar form of a propagating plane wave with a slowly varying envelope and phase

$$\vec{\mathcal{E}}(x, t) = \vec{\mathcal{E}}_0(x, t) \cos[\omega t - kx + \varphi(x, t)]. \quad (2.2)$$

The carrier frequency ω is approximately equal

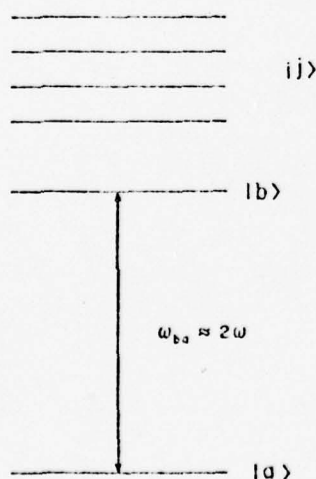


FIG. 1. Schematic energy-level diagram for an active atom. The energy separation between the states $|a\rangle$ and $|b\rangle$ is approximately twice the energy of an incident photon. The symbol $|j\rangle$ collectively represents all the intermediate states.

to one-half the atomic transition frequency $\omega_{ba} = (E_b - E_a)/\hbar$. We classify this situation as degenerate to distinguish it from the more general case in which two fields of different frequencies, ω_1 and ω_2 ($\omega_1 + \omega_2 = \omega_{ba}$), are propagated through the medium. The dipole-moment operator is assumed to have the form

$$\vec{p} = \sum_j |a\rangle\langle j| \vec{p}_{aj} + |b\rangle\langle j| \vec{p}_{bj} + (\text{hermitian adjoint}). \quad (2.3)$$

The coupling terms between intermediate states, i.e., terms of the form $|j\rangle\langle j'| \vec{p}_{jj'}$, are neglected in Eq. (2.3) since, under the present conditions, the atomic population is expected to be distributed only between the two active levels $|a\rangle$ and $|b\rangle$.

Our calculation is based on the traditional self-consistent approach. We construct equations of motion for the relevant atomic amplitudes C_a and C_b driven by the applied electric field. We then derive an expression for the atomic polarization in terms of the atomic amplitudes, and require, self-consistently, that the polarization act as a source term for the classical field-propagation equations. This approach was adopted to the description of a one-photon amplifier by Arecchi and Bonifacio.² Their results will be recalled in our discussion to emphasize the similarities and the differences between the one- and two-photon amplifier theories.

Our starting point is the Schrödinger equation,

$$i\hbar \frac{\partial}{\partial t} |\psi(t)\rangle = H |\psi(t)\rangle, \quad (2.4)$$

for a typical atom described by a state vector

$$|\psi(t)\rangle = \sum_j C_j(t) e^{-iE_j t/\hbar} |j\rangle + C_a(t) e^{-iE_a t/\hbar} |a\rangle + C_b(t) e^{-iE_b t/\hbar} |b\rangle. \quad (2.5)$$

The atomic state vector evolves under the action of the total Hamiltonian given by Eqs. (2.2) and (2.3). The atomic amplitudes C_j , C_a , C_b are assumed to be slowly varying in time, i.e., to reflect only the secular variations of the state vector. This assumption is well justified for single-photon processes under resonance conditions. In this case, in addition to requiring that $\omega \approx \frac{1}{2}\omega_{ba}$, we must neglect competing radiative processes which cause the atom to radiate at a different frequency from that of the stimulating field. In the presence of a strong signal at frequency ω this assumption appears justified.

The exact coupled equations for the atomic amplitudes are

$$\begin{aligned}
i\hbar\dot{C}_a(t) &= - \sum_j \mu_{aj} \mathcal{E}(x, t) C_j(t) e^{-i\omega_{ja}t}, \\
i\hbar\dot{C}_b(t) &= - \sum_j \mu_{bj} \mathcal{E}(x, t) C_j(t) e^{-i\omega_{jb}t}, \\
i\hbar\dot{C}_j(t) &= - \mu_{ja} \mathcal{E}(x, t) C_a(t) e^{i\omega_{ja}t} \\
&\quad - \mu_{jb} \mathcal{E}(x, t) C_b(t) e^{i\omega_{jb}t},
\end{aligned} \quad (2.6)$$

where we have assumed the field to be linearly polarized and where the dipole matrix elements μ_{ja} and μ_{jb} are projections along the direction of polarization of the field.

Our objective is to derive a set of coupled equations for the coherent amplitudes C_a and C_b . To this purpose we solve formally for the intermediate amplitudes $C_j(t)$ and replace Eqs. (2.6) by a pair of coupled integrodifferential equations for $C_a(t)$ and $C_b(t)$. The result is

$$\begin{aligned}
i\hbar\dot{C}_a(t) &= - \sum_j \mu_{aj} \mathcal{E}(x, t) e^{-i\omega_{ja}t} \\
&\quad \times \frac{i}{\hbar} \int_0^t dt' [\mu_{ja} \mathcal{E}(x, t') C_a(t') e^{i\omega_{ja}t'} \\
&\quad + \mu_{jb} \mathcal{E}(x, t') C_b(t') e^{i\omega_{jb}t'}].
\end{aligned} \quad (2.7)$$

A similar equation for $C_b(t)$ can be obtained from Eq. (2.7) by interchanging the indices a and b with one another. In order to reduce the exact integrodifferential equations to a manageable form, we perform the slowly varying amplitude approximation for both the atomic amplitudes and for the field envelope. This amounts to replacing $\mathcal{E}(x, t')$, $C_a(t')$, and $C_b(t')$ inside the integral with their values at the upper limit of integration, and carrying out the exact integration of the remaining exponential factors.

Upon retaining only the slowly varying terms, the required coupled equations for the atomic amplitudes $C_a(t)$ and $C_b(t)$ take the form

$$\begin{aligned}
\dot{C}_a(t) &= (i/\hbar) [k_{aa} |E_0|^2 C_a(t) + k_{ab} E_0^2 C_b(t) e^{i(\omega - \omega_{ba})t}], \\
\dot{C}_b(t) &= (i/\hbar) [k_{bb} |E_0|^2 C_b(t) + k_{ba} E_0^2 C_a(t) e^{-i(\omega - \omega_{ba})t}],
\end{aligned} \quad (2.8)$$

where the parameters k_{aa} , k_{bb} , and k_{ab} are given by

$$\begin{aligned}
k_{aa} &= \frac{2}{\hbar} \sum_j \mu_{ja}^2 \frac{\omega_{ja}}{\omega_{ja}^2 - \omega^2}, \\
k_{bb} &= \frac{2}{\hbar} \sum_j \mu_{jb}^2 \frac{\omega_{jb}}{\omega_{jb}^2 - \omega^2}, \\
k_{ab} &= \frac{1}{\hbar} \sum_j \frac{\mu_{ja} \mu_{jb}}{\omega_{ja}^2 - \omega^2},
\end{aligned} \quad (2.9)$$

and where the slowly time-varying field amplitude E_0 is defined by

$$\begin{aligned}
\mathcal{E}(x, t) &= \mathcal{E}_0(x, t) \cos[\omega t - kx + \varphi(x, t)] \\
&= E_0(x, t) e^{i\omega t} + E_0^*(x, t) e^{-i\omega t},
\end{aligned} \quad (2.10)$$

$$E_0(x, t) = \frac{1}{2} \mathcal{E}_0(x, t) e^{-i(\omega t - \varphi)}.$$

As an internal consistency check of the elimination of the intermediate amplitudes, we observe that

$$\frac{d}{dt} (|C_a|^2 + |C_b|^2) = 0 \quad (2.11)$$

as one must expect from probability-conservation requirements.

Within the approximations leading to the system of Eq. (2.8), we have replaced the exact dynamical evolution of the multilevel atom with a description that bears considerable similarity to the traditional analysis of a two-level system. The major difference, of course, is that Eqs. (2.8) contain the square of the field envelope, rather than the first power of the field as in the usual description of one-photon processes in a two-level system.

Next, we derive an expression for the atomic polarization in terms of the relevant amplitudes C_a and C_b . From the definition

$$P = N \langle p \rangle = N \langle \hat{p}(t) | p | \hat{\rho}(t) \rangle \quad (2.12)$$

and the operator representation (2.3) for the atomic dipole moment we find, as expected, that the total polarization depends on the entire set of atomic amplitudes, i.e.,

$$P = N \left(\sum_j \mu_{ja} C_a C_j^* e^{i\omega_{ja}t} + \sum_j \mu_{jb} C_b C_j^* e^{i\omega_{jb}t} + \text{c.c.} \right). \quad (2.13)$$

The elimination of the intermediate amplitudes $C_j(t)$ is carried out in identical fashion as in the derivation of the equations of motion (2.8). Thus, we replace $C_j(t)$ with their formal solution in terms of $C_a(t)$ and $C_b(t)$ and carry out the time integration after making the slowly-varying-amplitude approximation. The result of this calculation reveals polarization terms which oscillate at frequency ω , as well as terms oscillating at frequencies ω_{ja} , ω_{jb} , and at the third harmonic of the incident frequency. Thus, as already remarked (Grishchowsky *et al.* in Ref 5), competing effects may accompany two-photon emission or absorption processes.

In the presence of an injected field at frequency ω , it appears reasonable to ignore all the polarization contributions other than those which oscillate at the frequency of the externally injected pulse. In this case, the atomic polarization takes the form

$$P = N[k_{a1}|C_a|^2 + k_{b1}|C_b|^2 + k_{a2}(C_a C_b^* e^{-i\alpha} + C_a^* C_b e^{i\alpha})]S_0(x, t) \cos[\omega t - kx + \varphi(x, t)] \\ + Nk_{a2}i(C_a C_b^* e^{-i\alpha} - C_a^* C_b e^{i\alpha})S_0(x, t) \sin[\omega t - kx + \varphi(x, t)], \quad (2.14)$$

where

$$\alpha = (2\omega - \omega_{ba})t - 2kx + 2\varphi(x, t). \quad (2.15)$$

It is apparent from Eq. (2.14) that, as in the one-photon case, the induced atomic polarization contains terms that oscillate in-phase and terms that oscillate in quadrature with the applied field. The in-phase component of the polarization in Eq. (2.14), however, depends not only on bilinear terms of the type $C_a C_b^*$, but also on the populations of the active levels through C_a^2 and C_b^2 .

By analogy with the Bloch-vector representation of the one-photon theory, it is convenient to introduce the new atomic variables

$$R_1 = i(C_a C_b e^{i\alpha} - C_a^* C_b^* e^{-i\alpha}), \\ R_2 = -(C_a C_b^* e^{-i\alpha} + C_a^* C_b e^{i\alpha}), \quad (2.16) \\ R_3 = |C_b|^2 - |C_a|^2.$$

The physical meaning of R_3 and R_1 is immediately obvious: R_3 represents the population difference between the two levels of interest, while R_1 is proportional to the quadrature component of the nonlinear polarization. R_2 , however, is no longer proportional to the in-phase component of the polarization because of the dependence of $P(x, t)$ on the atomic populations.

In terms of the new variables, the atomic evolution is described by the set of equations

$$\dot{R}_1 = \left[\frac{k_{b1} - k_{a1}}{4\hbar} S_0^2 + \left(2\omega - \omega_{ba} + 2\frac{\partial\varphi}{\partial t} \right) R_2 + \frac{k_{a2}}{2\hbar} S_0^2 R_3, \right. \\ \dot{R}_2 = - \left[\frac{k_{b1} - k_{a1}}{4\hbar} S_0^2 + \left(2\omega - \omega_{ba} + 2\frac{\partial\varphi}{\partial t} \right) R_1, \quad (2.17) \\ \left. \dot{R}_3 = - \frac{k_{a2}}{2\hbar} S_0^2 R_1, \right]$$

while the atomic polarization takes the form

$$P = -Nk_{a2}S_0 \left[R_2 - \frac{k_{b1} - k_{a1}}{2k_{ab}} \left(R_3 + \frac{k_{a2} + k_{b2}}{k_{b1} - k_{a1}} \right) \right] \\ \times \cos(\omega t - kx + \varphi) - Nk_{a2}S_0 R_1 \sin(\omega t - kx + \varphi). \quad (2.18)$$

The conservation probability (2.11) is mapped into the conservation of the length of the Bloch vector

$$\frac{d}{dt}(R_1^2 + R_2^2 + R_3^2) = 0 \quad (2.19)$$

which follows at once from Eqs. (2.17).

On comparing Eqs. (2.17) with the usual Bloch equations for a two-level system we note two major differences: in Eqs. (2.17) the atomic variables

are driven by the square of the electric field envelope, rather than by the field envelope itself, and the detuning variable contains an intensity-dependent contribution. The immediate consequence of the latter feature is that, even in resonance ($2\omega = \omega_{ba}$ and $\partial\varphi/\partial t = 0$), the second component R_2 of the Bloch vector does not vanish for all time. This factor will be shown explicitly and discussed in Sec. III.

III. COUPLED SCHRÖDINGER-MAXWELL EQUATIONS

The field evolution is described by the wave equation

$$\frac{\partial^2}{\partial x^2} S - \frac{1}{c^2} \frac{\partial^2 S}{\partial t^2} = \frac{1}{c^2 \epsilon_0} \frac{\partial^2 P}{\partial t^2}. \quad (3.1)$$

In the slowly varying envelope and phase approximation Eq. (3.1) is equivalent to

$$S_0 \left(c \frac{\partial}{\partial x} + \frac{\partial}{\partial t} \right) \varphi = - \frac{\omega}{2\epsilon_0} P_c, \quad (3.2)$$

$$c \left(\frac{\partial}{\partial x} + \frac{\partial}{\partial t} \right) S_0 = - \frac{\omega}{2\epsilon_0} P_s, \quad (3.3)$$

where P_c and P_s are the in-phase and in-quadrature components of the polarization in Eq. (2.18). In terms of the atomic variables, the field equations (3.2) and (3.3) can be cast into the form

$$\left(c \frac{\partial}{\partial x} + \frac{\partial}{\partial t} \right) \left(2\omega - \omega_{ba} + 2\frac{\partial\varphi}{\partial t} \right) \\ = \frac{\omega N k_{a2}}{\epsilon_0} \left(\dot{R}_2 - \frac{k_{b1} - k_{a1}}{2k_{ab}} \dot{R}_3 \right), \quad (3.4)$$

$$\left(c \frac{\partial}{\partial x} + \frac{\partial}{\partial t} \right) S_0^2 = \frac{\omega N k_{a2}}{\epsilon_0} R_1 S_0^2. \quad (3.5)$$

The coupled set of equations (2.17), (3.4), and (3.5) represent the starting point of our analysis.

It is convenient to introduce the following notations

$$\gamma = (k_{b1} - k_{a1})/2k_{ab}, \quad g = \omega N k_{a2}/\epsilon_0, \\ \omega_R = (1 + \gamma^2)^{1/2} (k_{a2}/2\hbar) S_0^2, \quad (3.6)$$

$$\Omega = (2\omega - \omega_{ba}) + 2\frac{\partial\varphi}{\partial t},$$

and to refer the atom-field evolution to the local coordinate frame

$$\eta = x/c, \quad \tau = t - x/c. \quad (3.7)$$

The coupled Schrödinger-Maxwell equations can be written in the form

$$\begin{aligned}\frac{\partial R_1}{\partial t} &= \left(\frac{\gamma}{(1+\gamma)^{1/2}} \omega_R + \Omega \right) R_2 + \frac{\omega_R}{(1+\gamma)^{1/2}} R_3, \\ \frac{\partial R_2}{\partial t} &= - \left(\frac{\gamma}{(1+\gamma)^{1/2}} \omega_R + \Omega \right) R_1,\end{aligned}\quad (3.8)$$

$$\begin{aligned}\frac{\partial R_3}{\partial t} &= - \frac{\omega_R}{(1+\gamma)^{1/2}}; \\ \frac{\partial \omega_R}{\partial \eta} &= g \omega_R R_1 - l \omega_R, \\ \frac{\partial \Omega}{\partial \eta} &= g \left(\frac{\partial R_2}{\partial \tau} - j \frac{\partial R_1}{\partial \tau} \right).\end{aligned}\quad (3.9)$$

The field-envelope equation is written in terms of the "Rabi frequency" ω_R which is proportional to the square of the field envelope. The damping term $-l\omega_R$ has been added phenomenologically to describe the effects of nonresonant losses.

In the coherent propagation limit, i.e., neglecting atomic relaxation effects, the field equation can be cast into the form

$$\begin{aligned}\frac{\partial \omega_R}{\partial t} &= g \omega_R R_1 - l \omega_R, \\ \frac{\partial \Omega}{\partial \eta} &= -g \Omega R_1,\end{aligned}\quad (3.10)$$

which reveal an interesting conservation relation for the product of the Rabi frequency ω_R and the detuning Ω . In fact, from Eqs. (3.10), we find

$$\frac{\partial}{\partial \eta} (\omega_R \Omega) = -l \omega_R \Omega. \quad (3.11)$$

Equation (3.11) can be integrated at once to yield

$$(\omega_R \Omega)_\eta = (\omega_R \Omega)_{\eta=0} e^{-l\eta}. \quad (3.12)$$

If at the input of the active medium the detuning parameter is zero, it remains identically zero, everywhere. We define as resonant propagation the situation in which $\Omega=0$ for all values of η . In this case a closed-form solution exists for the atomic variables R_1 , R_2 , and R_3 which is easily shown to be (see e.g., Belenov *et al.* in Ref. 3)

$$\begin{aligned}R_1 &= [R_1^0 / (1+\gamma^2)^{1/2}] \sin \sigma, \\ R_2 &= [R_3^0 / (1+\gamma^2)^{1/2}] (\cos \sigma - 1), \\ R_3 &= [R_3^0 / (1+\gamma^2)] (\cos \sigma + \gamma^2),\end{aligned}\quad (3.13)$$

where R_i^0 is the population difference $|c_b|^2 - |c_a|^2$ just prior to the arrival of the leading edge of the pulse at a given depth into the active (or absorbing) medium.

In arriving at Eqs. (3.13) we have assumed implicitly the swept excitation initial conditions

$$\begin{aligned}R_1(\tau=0, \eta) &= 0, \\ R_2(\tau=0, \eta) &= 0, \\ R_3(\tau=0, \eta) &= R_3^0.\end{aligned}\quad (3.14)$$

The parameter $\sigma(\eta, \tau)$ is related to the Rabi frequency by the simple relation

$$\frac{\partial \sigma(\eta, \tau)}{\partial \tau} = \omega_R \quad (3.15)$$

or by

$$\sigma(\eta, \tau) = \int_0^\tau d\tau' \omega_R(\eta, \tau'). \quad (3.16)$$

Hence, σ is proportional to the integrated pulse energy from the leading edge of the pulse up to a given value τ of the local time. The total pulse energy will be denoted by

$$\Sigma(\eta) = \lim_{\tau \rightarrow \infty} \sigma(\eta, \tau); \quad (3.17)$$

It is easy to derive the equation of motion for $\sigma(\eta, \tau)$. From the first field equation (3.10) and from Eq. (3.13) we have

$$\frac{\partial^2 \sigma}{\partial \eta \partial \tau} = \frac{g}{(1+\gamma^2)^{1/2}} \sin \sigma \frac{\partial \sigma}{\partial \tau} - l \frac{\partial \sigma}{\partial \tau}. \quad (3.18)$$

We find a major difference between Eq. (3.18) and the "area" equation derived by Arecchi and Bonifacio for a one-photon amplifier. The Arecchi-Bonifacio area equation has the form

$$\frac{\partial^2 \sigma}{\partial \eta \partial \tau} = G \sin \sigma - l \frac{\partial \sigma}{\partial \tau}, \quad (3.19)$$

where σ represents the area under the electric field envelope. In our case the nonlinear driving term on the right-hand side of Eq. (3.18) contains the product $\sin \sigma (\partial \sigma / \partial \tau)$. This circumstance allows us to make general statements concerning the behavior of the pulse energy which are drastically different from those derived for a one-photon amplifier.

In order to analyze the spatial variation of the pulse energy, we integrate Eq. (3.18) with respect to the local time τ . Upon taking the limit $\tau \rightarrow \infty$, we have

$$\frac{\partial}{\partial \eta} \Sigma(\eta) = -l \Sigma(\eta) + \frac{g}{(1+\gamma^2)^{1/2}} [1 - \cos \Sigma(\eta)]. \quad (3.20)$$

The solution of Eq. (3.20) in the lossless case ($l=0$) is found to be

$$\Sigma(\eta) = 2 \arccot \left(\cotan \frac{1}{2} \Sigma(0) - \frac{g}{(1+\gamma^2)^{1/2}} \eta \right) + 2k\pi \quad (3.21a)$$

or

$$\Sigma(\eta) = 2 \arccot \left(\cotan \frac{1}{2} \Sigma(0) - \frac{g}{(1+\gamma^2)^{1/2}} \eta \right) + 2(k+1)\pi \quad (3.21b)$$

where (3.21a) applies when the expression in large parentheses is positive, and (3.21b) when it is ne-

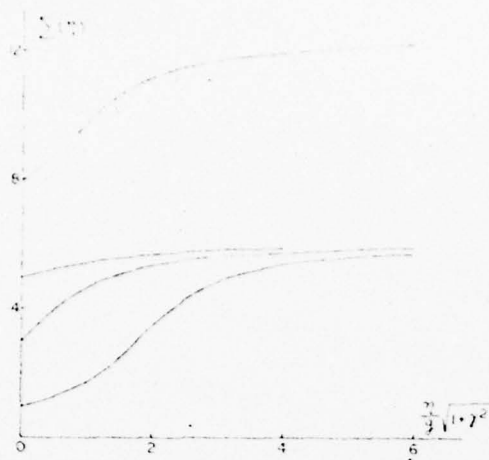


FIG. 2. Spatial behavior of the pulse energy $\Sigma(\eta)$ (Eqs. (3.21a) and (3.21b)) for different values of the input value $\Sigma(0)$.

gative. The integer number k equals the integral part of $\Sigma(0)/2\pi$, and $\Sigma(0)$ is proportional to the input pulse energy.

Typical solutions are shown in Fig. 2 corresponding to different input energies $\Sigma(0)$. It is obvious both from Eq. (3.20) and from the solutions in Fig. 2 that the efficiency of the amplifier, measured for example in terms of the initial rate of growth, is not a monotonic function of the input energy, as in the case of an ordinary amplifier. The initial rate of growth, instead, is maximum for $\Sigma(0) = \pi$ and odd multiples of π , while it vanishes for $\Sigma(0) = 2\pi, 4\pi$, etc. In the latter case the pulse energy is conserved during the propagation.

Detailed information about the pulse envelope cannot be obtained from Eq. (3.20). A computer simulation of Eqs. (3.8) and (3.10) has shown that, even when the pulse energy is conserved during the evolution, pulse reshaping takes place with a continuous narrowing of the pulse and a subsequent growth of the peak power.

Interesting predictions can be made also about the asymptotic behavior ($\eta \rightarrow \infty$) of a pulse even when the field losses are taken into account ($l \neq 0$). In this case the asymptotic solution $\Sigma(\infty)$ must satisfy the transcendental equation

$$1 - \cos \Sigma(\infty) = (1 + \gamma^2)^{1/2} (l/g) \Sigma(\infty). \quad (3.22)$$

It is apparent that multiple steady-state solutions are possible. Three typical situations are indicated in Fig. 3. With reference to this figure, the straight line labeled 1 corresponds to $(1 + \gamma^2)^{1/2} l/g = 1$. The only solution of Eq. (3.22) in this case is $\Sigma(\infty) = 0$. The pulse is completely dissipated by the scattering losses and no energy or power simplifi-

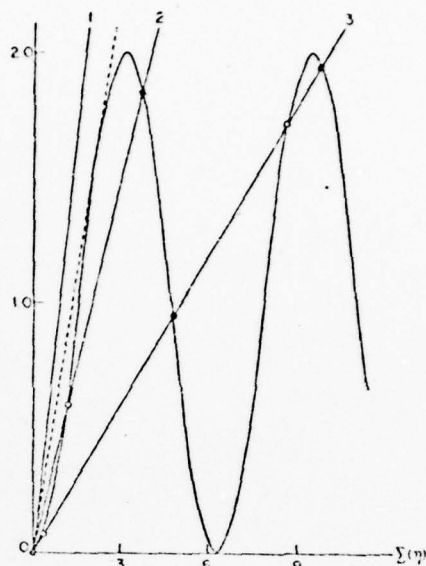


FIG. 3. Asymptotic steady-state solutions of the area equation [Eq. (3.20)] correspond to the intercepts of the straight lines $(1 + \gamma^2)^{1/2} (l/g) \Sigma(\eta)$ with the curve $1 - \cos \Sigma(\eta)$. The straight lines 1, 2, and 3 have slopes equal to 1, $\frac{1}{2}$, and $\frac{1}{3}$, respectively. The stable solutions are marked with solid circles. The unstable solutions are marked with open circles. The critical slope (dashed line) is 0.7246.

cation is possible in the inverted medium. The straight line labeled 2 corresponds to $(1 + \gamma^2)^{1/2} l/g = \frac{1}{2}$. It intersects the curve $1 - \cos \Sigma(\infty)$ in three points. It is trivial to verify from Eq. (3.20) that the intercepts marked with solid circles represent possible stable solutions, whereas the intercept marked with an open circle is an unstable asymptotic solution. In the case of the straight line labeled 3, we have chosen $(1 + \gamma^2)^{1/2} l/g = \frac{1}{3}$. Three possible stable solutions exist [one corresponding to the trivial case $\Sigma(\infty) = 0$].

Several conclusions can be gathered from the above observations.

(i) Two simultaneous requirements must be satisfied for the asymptotic propagation of a pulse with an energy $\Sigma(\infty) \neq 0$. First, the parameter $(1 + \gamma^2)^{1/2} \times l/g$ must be smaller than the absolute critical value 0.7246. (The slope of the dashed line in Fig. 2.) Secondly, the incident pulse energy must be larger than the value of Σ corresponding to the first unstable root for a given choice of $(1 + \gamma^2)^{1/2} l/g$. If both conditions are satisfied, the total pulse energy will converge to a stable nonvanishing value.

(ii) The output of the pulse energy can be larger or smaller than its input value $\Sigma(0)$ depending on the magnitude of $\Sigma(0)$ relative to the nearest stable solution $\Sigma(\infty)$. This aspect of the propagation prob-

lem will be confirmed by our computer simulations where it is seen that power amplification in the coherent regime can occur both with energy amplification or reduction.

(iii) There is no small signal gain; i.e., even if the parameter $(1+\gamma^2)^{1/2}/g$ is sufficiently small an input signal with energy smaller than the first unstable root will not be amplified.

(iv) It is anticipated that whenever multiple stable solutions are possible, the n th stable root $\Sigma(\infty)$ corresponds to a pulse envelope that has been split into $n-1$ distinct pulses (see Fig. 6).

In addition to the above remarks, we can add that the field equations (3.10) do not allow a steady-state solution for the pulse envelope. This feature is confirmed by our computer simulations where it is seen that, when the threshold conditions are satisfied, the peak power continues to grow and the pulse duration becomes smaller and smaller, as the pulse energy approaches its stable asymptotic value.

IV. COMPUTER SIMULATION STUDIES

The coupled set of equations (3.2) and (3.10) has been analyzed with a hybrid computer in the limiting case of resonant interaction and with the atomic system prepared in a swept excitation mode corresponding to the initial conditions (3.4), and to the boundary conditions

$$\Omega(\eta=0, \tau)=0 \quad \omega_R(\eta=0, \tau)=\omega_R(\tau). \quad (4.1)$$

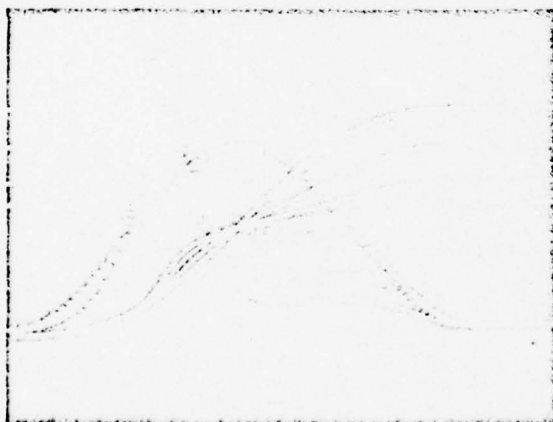


FIG. 4. Computer simulation illustrating the evolution of the pulse intensity through the amplifying medium. The different dashed curves represent the intensity envelope in different sections of the amplifier. The solid curves are the corresponding integrated energy $\sigma(\eta, \tau)$. The value of $\sigma(\eta, \infty)$ at the far right gives the total energy $\Sigma(\eta)$. The horizontal axis is the local time axis with $\tau=0$ (leading edge of the input) at the far left. The input energy is $\Sigma(0)=4$ and the gain-to-loss ratio $g/(1+\gamma^2)^{1/2}=2$. Note the transient envelope modulation.

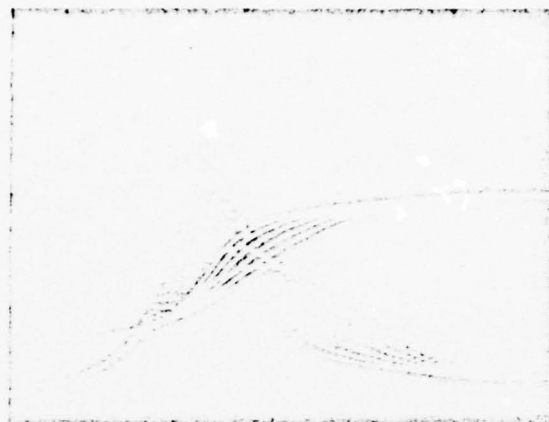


FIG. 5. Evolution of a pulse with an initial energy very close to the expected asymptotic stable value. The input energy is $\Sigma(0)=5$ and the gain-to-loss ratio is 5.

The input pulse envelope has the form

$$\omega_R(\tau) = \omega_R^0 \sin^2(\pi\tau/\tau_p), \quad (4.2)$$

where τ_p denotes the pulse duration from the leading to the trailing edge.

As expected the detuning parameter Ω remains identically equal to zero throughout the evolution of the pulse, an indication that the computer round-off error has been kept small. An additional check of the accuracy of the solution is provided by the conserved nature of the linear combination of atomic variables $R_2 - \gamma R_3$ as one can verify at once from Eq. (3.8) in the resonant case. We have monitored $R_2 - \gamma R_3$, and found it to be essentially constant over the entire range of integration of the problem.

Figures 4-6 show some typical solutions of the

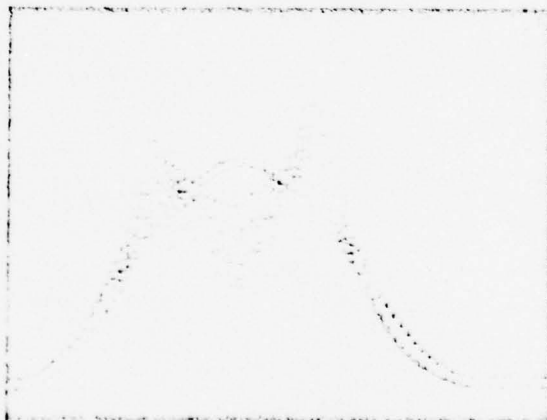


FIG. 6. Pulse splitting and double pulse propagation in the coherent limit. The input energy is $\Sigma(0)=9.8$ and the gain-to-loss ratio is 5.

propagation problem. The dotted lines represent successive pulse shapes at various sections along the amplifier, while the solid lines give the corresponding pulse energies $\sigma(p, \tau)$. As shown in Sec. III the input energy $\Sigma(0)$ and the gain-to-loss ratio $g/l(1+\gamma)^{1/2}$ control the asymptotic behavior of the pulse energy under coherent propagation conditions. In Fig. 4 the gain to loss ratio equals 2. As shown in Fig. 3, only one steady-state value of $\Sigma(\infty)$ is possible corresponding to the present choice of $g/l(1+\gamma)^{1/2}$ provided $\Sigma(0)$ exceeds its threshold value. This behavior is confirmed by the solution shown in Fig. 4. In addition, the initial energy $\Sigma(0)$ is larger than the predicted asymptotic value for the chosen gain to loss ratio. As a result the pulse energy decreases monotonically as the pulse envelope reshapes itself.

In Fig. 5, we display the evolution of a pulse with an initial energy $\Sigma(0)=5$ propagating in a medium with a gain-to-loss ratio equal to 5. In this case two steady-state values of $\Sigma(\infty)$ are possible. Corresponding to the chosen initial value of $\Sigma(0)$, the solution evolves into a single narrow pulse with

an asymptotic energy that can be read off directly from Fig. 3.

In Fig. 6, we show the effect of increasing the incident pulse energy while keeping the gain-to-loss ratio equal to 5, as in the previous case. The envelope reshapes into two separate pulses which appear to evolve more or less independently.

Additional solutions obtained for larger values of the gain-to-loss ratio have confirmed that the n th stable energy $\Sigma(\infty)$ corresponds to a pulse envelope that has split into $n-1$ separate pulses.

Further work to incorporate the effects of detuning and irreversible atomic relaxation is in progress.

ACKNOWLEDGMENTS

One of us (L.M.N.) wishes to express his appreciation to Professor Rodolfo Bonifacio for a very informative conversation. The support and encouragement of the Quantum Physics, Physical Sciences Directorate at Redstone Arsenal, Alabama, and especially of R. A. Shates and Dr. C. M. Bowden, is gratefully acknowledged.

*Work partially supported by the Army Research Office Grant No. DAAG29-76-G-0075 and by the ONR Contract No. N0014-76-C-1032.

¹A. M. Prokhorov, *Science* **149**, 823 (1965).

²P. P. Sorokin, N. Brashin, *IBM J. Res. Dev.* **8**, 177 (1964).

³S. R. Hartmann, *IEEE J. Quant. Electron.* **QE-4**, 802 (1968); E. M. Belenov and I. A. Poluektov, *Sov. Phys. JETP* **22**, 754 (1969); M. Takatsuji, *Physica (Utr.)* **51**, 265 (1971); *Phys. Rev. B* **2**, 340 (1970); D. Grischowski, *Phys. Rev. Lett.* **24**, 866 (1970); N. Tan-no, K. Yokoto, and H. Inaba, *Phys. Rev. Lett.* **29**, 1211 (1972).

⁴For a critical comparison of the different theoretical approaches see, for example, D. Grischowski, in *Laser Applications to Optics and Spectroscopy*, Vol. II of *Physics of Quantum Electronics Series*, edited by S. F. Jacobs, M. Sargent, III, J. F. Scott,

and M. O. Scully (Addison-Wesley, Reading, Mass., 1975).

⁵N. Tan-no, K. Yokoto, and H. Inaba, *J. Phys. B* **8**, 359 (1975); **8**, 349 (1975); M. Takatsuji, *Phys. Rev. A* **11**, 619 (1975); D. Grischowski, M. M. T. Loy, and P. F. Liao, *ibid.* **12**, 2514 (1975); R. Brewer and E. L. Hahn, *ibid.* **11**, 1611 (1975).

⁶R. L. Shoemaker and R. G. Brewer, *Phys. Rev. Lett.* **28**, 1430 (1972); N. Tan-no, K. Yokoto, and H. Inaba, *ibid.* **19**, 1211 (1972); H. Nakatsuka, J. Okada, and M. Matsuoka, *J. Phys. Soc. Jpn.* **37**, 1406 (1974).

⁷L. E. Estes, L. M. Narducci, and B. Shammah, *Nuovo Cimento Lett.* **1**, 175 (1971).

⁸R. L. Carman, *Phys. Rev. A* **12**, 1048 (1974).

⁹F. T. Arecchi and R. Bonifacio, *IEEE J. Quant. Electr.* **QE-1**, 169 (1965).

¹⁰S. L. McCall and E. L. Hahn, *Phys. Rev. Lett.* **18**, 1019 (1967).

Reprinted from: COHERENCE IN SPECTROSCOPY AND MODERN PHYSICS
Edited by E. T. Arecchi, R. Bonifacio, and M. O. Scully
Book available from: Plenum Publishing Corporation
227 West 17th Street, New York, N. Y. 10011

COHERENT TWO-PROTON AMPLIFICATION IN AN INVERTED MEDIUM*

L.M. Narducci, L.C. Johnson, E.J. Seibert, W.W. Eidson

Department of Physics and Atmospheric Science
Drexel University
Philadelphia, Pennsylvania 19104

Abstract: We study the propagation of an electromagnetic pulse in an inverted medium where atomic levels of interest have the same parity and an energy separation equal to twice the energy of the incident photons. We analyze the coupled atom-field evolution equations in the limit when incoherent atomic relaxation processes can be neglected, and derive the threshold conditions for amplification and a few exact conservation relations. The detailed evolution of the pulse through the inverted medium is investigated with the help of a hybrid computer.

1. INTRODUCTION

The subject matter of these lectures concerns the interaction of coherent electromagnetic radiation and matter. This problem of course, has played a central role in Quantum Optics and continues to be of great current interest as indicated by the numerous recent advances discussed in this volume. In the traditional view of radiation-matter interaction, the atoms are pictured as two-level systems undergoing transitions between dipole-coupled energy levels¹. Our setting, instead, will be substantially different.

The two active levels in our medium are assumed to have the same parity. All the other energy levels play the role of virtual states in the atomic dynamics. Because no direct transitions are allowed between the two levels of interest,

*Work partially supported by the Office of Naval Research contract number N00014-76-C-1082.

spontaneous or stimulated emission of radiation must be provided by other processes such as, for example, inelastic atomic collisions, spontaneous decay through a ladder of lower lying states, or higher-order non-linear effects induced by an external field.

The latter mechanism and, in particular, the two-photon emission process will be explored in these lectures as a means for producing amplification of an incident pulse of radiation.

Two-photon transitions have been the subject of considerable activity in the last few years², yielding for example, such spectacular pay-offs as Doppler-free spectroscopy³. Early in the development of the theory of two-photon processes considerable interest was directed to the study of coherent atomic evolution⁴. As a result of these efforts, many well known one-photon coherent atomic effects were shown to have two-photon analogues⁵.

Much of the recent work has focused on the evolution of atoms from their ground state. More limited attention has been paid to the propagation of an incident pulse in an inverted medium⁶. We address ourselves to this problem with the added restriction that the carrier frequency of the incident pulse be approximately one half the atomic transition frequency. The more general situation involving two incident pulses whose carrier frequencies add up to the atomic transition frequency has also been considered in the literature⁷. This generalization, however, will not be discussed in these lectures.

Our analysis evolves along the lines mapped out by Estes et al. in the context of the so-called self-consistent field approximation⁸. Schematically, one can picture the process as follows: the incident field drives the excited atoms and generates a non-linear polarization which oscillates with a carrier frequency equal to that of the incident field. The radiated and incident fields add coherently and drive another group of atoms further down into the active medium. This picture is oversimplified because additional non-linear polarization components also come into play and competition effects may become important. Additional comments on this problem will be made in subsequent sections of this paper.

Mathematically, the atomic evolution is described by the Schrödinger equation; the field propagation, instead, is governed by Maxwell's equations. The macroscopic non-linear polarization is calculated self-consistently in terms of the quantum mechanical atomic amplitudes⁹.

The resulting atomic equations can be cast into a form that is formally identical to that of the familiar Bloch equations describing the one-photon evolution of two-level systems. Two main differences will be noted: the driving field amplitude enters quadratically, rather than linearly, in the atomic equations of motion, and intensity-dependent dispersion effects are predicted which will be interpreted as dynamic Stark shifts.

II. ATOMIC EVOLUTION

In order to fix our attention on a concrete example, consider the lowest lying levels of the singlet spectrum of Calcium (Fig. 1)

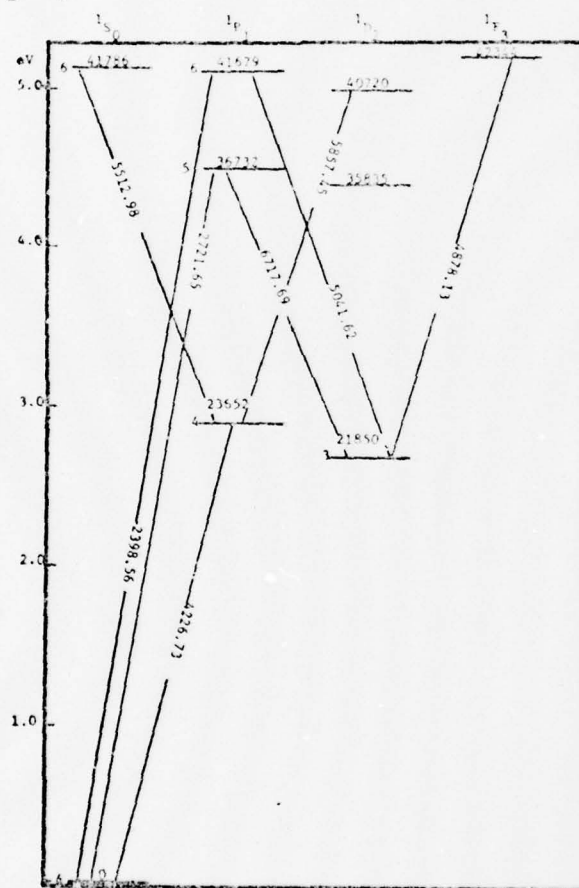


Figure 1. Lower lying singlet levels of Calcium

We assume the atoms to be initially prepared in a state of inversion between the 1D_2 level at 21850 cm^{-1} and the ground state. The 1D_2 level is the lowest excited state of the singlet manifold. It is weakly coupled to the ground state by a quadrupole transition, and to lower lying triplet states by collisional mixing. The absence of lower lying P states is an important practical advantage of Calcium atoms, if one wants to maintain a sufficient inversion prior to the arrival of the signal to be amplified.

The schematic energy level diagram to be kept in mind for the following development is illustrated in Fig. 2. The active levels $|a\rangle$ (e.g. the ground 1S_0 state) and $|b\rangle$ (e.g. the excited 1D_2 state) are separated by an energy difference $\hbar\omega_{ba}$ and are assumed to have identical parity. At the end of the pumping process an injected electromagnetic signal with carrier frequency approximately equal to $\frac{1}{2}\omega_{ba}$ is assigned the task of producing the required non-linear polarization between the active levels.

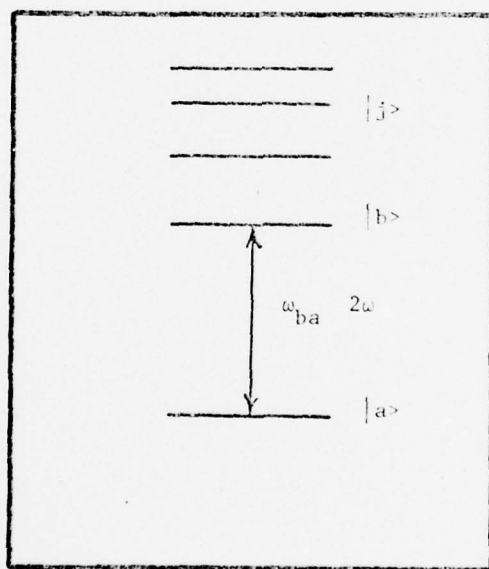


Figure 2. Schematic energy level diagram of the atomic model used in the calculations

With reference to Fig. 2, a typical atom is described by the state vector

$$|\psi(t)\rangle = \sum_j C_j(t) \exp(-iE_j t/\hbar) |j\rangle + C_a(t) \exp(-iE_a t/\hbar) |a\rangle + C_b(t) \exp(-iE_b t/\hbar) |b\rangle, \quad (2.1)$$

where the eigenvectors $|j\rangle$ refer to all the higher states of the atomic spectrum.

The atomic evolution is generated by the total Hamiltonian

$$H = E_a |a\rangle\langle a| + E_b |b\rangle\langle b| + \sum_j E_j |j\rangle\langle j| - p \mathcal{E}(x, t), \quad (2.2)$$

where p is the dipole moment operator in the direction of polarization of the incident field, and where $\mathcal{E}(x, t)$ is assumed to have the form of a propagating plane wave with a slowly varying envelope and phase:

$$\mathcal{E}(x, t) = \mathcal{E}_0(x, t) \cos(\omega t - kx + \varphi(x, t)), \quad (2.3)$$

The field carrier frequency ω is set approximately equal to $\frac{1}{2} \omega_{ba} = \frac{1}{2}(E_b - E_a)/\hbar$.

As a result of our assumption concerning the parity of the active levels, the dipole moment operator takes the form

$$p = \sum_j \mu_{aj} |a\rangle\langle j| + \mu_{bj} |b\rangle\langle j| + \text{hermitian adjoint}, \quad (2.4)$$

The coupling terms μ_{jj} , $|j\rangle\langle j|$ between intermediate states are ignored.

The exact Schrödinger equation for the state vector (2.1) is equivalent to an infinite hierarchy of coupled amplitude equations involving not only $C_a(t)$ and $C_b(t)$, but also the amplitudes of all the intermediate states $|j\rangle$. As a first step we need to eliminate the intermediate state amplitudes using the slowly varying amplitude approximation and the assumed quasi-resonance condition $2\omega \approx \omega_{ba}$. This program can be accomplished as indicated: we find the formal solution for $C_j(t)$ and eliminate the intermediate state amplitudes from the equations for $C_a(t)$ and $C_b(t)$. The result is a pair of coupled integro-differential equations of the type

$$\begin{aligned}
\hbar \frac{d}{dt} C_a(t) = & - \sum_j \mu_{aj} \mathcal{E}(x,t) \exp(-i\omega_{ja}t) \cdot \frac{i}{\hbar} \int_0^t dt' \\
& (\mu_{ja} \mathcal{E}(x,t') C_a(t') \exp(i\omega_{ja}t) + \mu_{jb} \mathcal{E}(x,t') C_b(t') \\
& \exp(i\omega_{jb}t')) , \quad (2.5)
\end{aligned}$$

(A similar equation for $C_b(t)$ follows from Eq. (2.5) upon interchanging the indices a and b with one another.)

The exact problem may now be reduced to manageable form by taking advantage of the slowly varying amplitude approximation. This amounts to replacing the field amplitude $\mathcal{E}_0(x,t')$ and the atomic amplitudes $C_a(t')$ and $C_b(t')$ inside the integral with their values at the upper limit of integration. Finally, the exact integration of the remaining exponential factors can be easily carried out. At this point, for consistency, only the secular terms must be retained.

As a result, the atomic amplitudes $C_a(t)$ and $C_b(t)$ are found to satisfy the coupled equations of motion

$$\begin{aligned}
\frac{d}{dt} C_a(t) = & \frac{i}{\hbar} \{ \frac{1}{2} k_{aa} \mathcal{E}_0^2 C_a(t) + \frac{1}{2} k_{ab} \mathcal{E}_0^2 C_b(t) e^{i\alpha} \} \\
\frac{d}{dt} C_b(t) = & \frac{i}{\hbar} \{ \frac{1}{2} k_{bb} \mathcal{E}_0^2 C_b(t) + \frac{1}{2} k_{ab} \mathcal{E}_0^2 C_a(t) e^{-i\alpha} \} , \quad (2.6)
\end{aligned}$$

The parameters

$$\begin{aligned}
k_{aa} = & \frac{2}{\hbar} \sum_j \mu_{ja}^2 \frac{\omega_{ja}}{\omega_{ja}^2 - \omega^2} \\
k_{bb} = & \frac{2}{\hbar} \sum_j \mu_{jb}^2 \frac{\omega_{jb}}{\omega_{jb}^2 - \omega^2} , \quad (2.7)
\end{aligned}$$

are the electric susceptibilities of a single atom in the states $|a\rangle$ and $|b\rangle$, respectively, and

$$k_{ab} = \frac{1}{\hbar} \sum_j \frac{\mu_{ja} \mu_{jb}}{\omega_{jb} + \omega} \quad (2.8)$$

is the so-called two-photon gyroelectric ratio.

The phase angle α is defined as

$$\alpha = (2\omega - \omega_{ba})t - 2kx + 2\psi(x,t). \quad (2.9)$$

As a check of the internal consistency of the elimination process, we observe that

$$\frac{d}{dt} (|c_a|^2 + |c_b|^2) = 0, \quad (2.10)$$

as one would expect from probability conservation arguments if the virtual states are not populated during the evolution.

The amplitude equations (2.6) bear a considerable similarity to those which govern the evolution of two-level atoms undergoing one-photon transitions¹. In the two-photon case, however, the field amplitude enters quadratically as one might expect in view of the nature of the atomic transition.

III. FIELD EQUATIONS

The field propagation in the medium is described by the wave equation in one dimension

$$\frac{\partial^2 \mathcal{E}}{\partial x^2} - \frac{1}{c^2} \frac{\partial^2 \mathcal{E}}{\partial t^2} = \frac{1}{c^2 \epsilon_0} \frac{\partial^2 P}{\partial t^2}, \quad (3.1)$$

where the source term P is the macroscopic polarization of the sample and ϵ_0 is the vacuum permittivity. A convenient representation for the macroscopic polarization is

$$P(x,t) = P_c \cos(\omega t - kx + \psi) + P_s \sin(\omega t - kx + \psi). \quad (3.2)$$

The in-phase (P_c) and out-of-phase (P_s) components of the polarization will be slowly varying functions of space and time if the carrier frequency of $P(x,t)$ is approximately the same as that of the driving field. In the presence of competing contributions oscillating at frequencies other than ω , the polarization components P_c and P_s will, of course, be no longer slowly varying. This issue will be discussed more at length in Section 4.

Within the slowly varying amplitude and phase approximation, Eq. (3.1) reduces to the following pair of coupled transport equations

$$\begin{aligned} \mathcal{E}_0 \left(c \frac{\partial}{\partial x} + \frac{\partial}{\partial t} \right) \psi &= - \frac{\omega}{2\epsilon_0} P_c, \\ \left(c \frac{\partial}{\partial x} + \frac{\partial}{\partial t} \right) \mathcal{E}_0 &= - \frac{\omega}{2\epsilon_0} P_s, \end{aligned} \quad (3.3)$$

which govern the propagation of the field amplitude \tilde{E}_0 and phase ψ .

IV. ATOMIC POLARIZATION

The equations of motion developed in Sections 2 and 3 are made self-consistent by calculating the polarization components P_x and P_y in terms of the quantum mechanical atomic amplitudes. By definition, the macroscopic polarization is given by

$$P = N \langle \psi(t) | p | \psi(t) \rangle \quad (4.1)$$

where p is the dipole moment operator (Eq. (2.4)), $|\psi(t)\rangle$ the atomic state vector (Eq. (2.1)), and N is the atomic number density. As expected, the total polarization depends on the entire set of atomic amplitudes, i.e.

$$P = N \left\{ \sum_j \mu_{ja} C_a C_j^* e^{i\omega_{ja}t} + \mu_{jb} C_b C_j^* e^{i\omega_{jb}t} + C.C. \right\} \quad (4.2)$$

Our immediate task is to eliminate the intermediate state amplitudes C_j consistently with the approximations made in deriving the atomic equations of motion (Eq. (2.6)). First we replace C_j in (Eq. (4.2)) with their exact formal solution, we replace the slowly varying amplitudes $\tilde{E}_0(x, t')$, $C_a(t')$ and $C_b(t')$ with their values at the upper limit of the time integrations, and carry out the remaining elementary integrals.

The result of the lengthy but simple calculation reveals polarization contributions that oscillate at a frequency ω , as well as terms oscillating at the frequencies ω_{ja} , ω_{jb} , and 3ω . These additional terms oscillating at the "wrong" frequencies open the door to competing effects which may accompany the two-photon absorption or emission processes. A detailed analysis of the third harmonic contribution has shown that it can be eliminated if the incident pulse is circularly polarized¹⁰. Raman type competitions, on the other hand cannot be ruled out. The question of their importance in this problem remains to be worked out in detail.

In the following development we retain only the polarization components that oscillate at the frequency of the incoming field. In this case, the atomic polarization takes the form

$$\begin{aligned}
 P = N \{ & k_{aa} |C_a|^2 + k_{bb} |C_b|^2 + k_{ab} (C_a C_b^* e^{-i\alpha} + C_a^* C_b e^{i\alpha}) \} \\
 & \mathcal{E}_0(x, t) \cos(\omega t - kx + \psi) \\
 & + N k_{ab} i (C_a C_b^* e^{-i\alpha} - C_a^* C_b e^{i\alpha}) \mathcal{E}_0(x, t) \sin(\omega t - kx + \psi)
 \end{aligned} \quad (4.3)$$

As in the one-photon case, the polarization depends on the expected bilinear combinations of atomic amplitudes (e.g. $C_a C_b^*$). In this case, however, the in-phase component depends also on the population of the active levels through $|C_a|^2$ and $|C_b|^2$.

V. COUPLED ATOM-FIELD EQUATIONS

By analogy with the Bloch vector representation of the one-photon theory^{1,9}, it is convenient to introduce the new atomic variables

$$\begin{aligned}
 R_1 &= i(C_a^* C_b e^{i\alpha} - C_a C_b^* e^{-i\alpha}) \\
 R_2 &= -(C_a C_b^* e^{-i\alpha} + C_a^* C_b e^{i\alpha}) \\
 R_3 &= |C_b|^2 - |C_a|^2
 \end{aligned} \quad (5.1)$$

This choice leads to the familiar looking vector form for the atomic equations

$$\begin{aligned}
 \dot{R}_1 &= \left[\frac{k_{bb} - k_{aa}}{4\hbar} \mathcal{E}_0^2 + (2\omega - \omega_{ba} + 2 \frac{\partial \psi}{\partial t}) \right] R_2 + \frac{k_{ab}}{2\hbar} \mathcal{E}_0^2 R_3 \\
 \dot{R}_2 &= - \left[\frac{k_{bb} - k_{aa}}{4\hbar} \mathcal{E}_0^2 + (2\omega - \omega_{ba} + 2 \frac{\partial \psi}{\partial t}) \right] R_1 \\
 \dot{R}_3 &= - \frac{k_{ab}}{2\hbar} \mathcal{E}_0^2 R_1
 \end{aligned} \quad (5.2)$$

The field equations take the form

$$\begin{aligned}
 (c \frac{\partial}{\partial x} + \frac{\partial}{\partial t}) \mathcal{E}_0^2 &= \frac{\omega N k_{ab}}{\epsilon_0} R_1 \mathcal{E}_0^2 \\
 (c \frac{\partial}{\partial x} + \frac{\partial}{\partial t}) (2\omega - \omega_{ba} + 2 \frac{\partial \psi}{\partial t}) &= \frac{\omega N k_{ab}}{\epsilon_0} (\dot{R}_2 - \frac{k_{bb} - k_{aa}}{2k_{ab}} \dot{R}_3)
 \end{aligned} \quad (5.3)$$

It is convenient to introduce the following notations

$$\gamma = \frac{k_{bb} - k_{aa}}{2k_{ab}}, \quad g = \frac{\omega N k_{ab}}{\epsilon_0}$$

$$\omega_R = \sqrt{1+\gamma^2} \frac{k_{ab}}{2\hbar} \mathcal{E}_0^2 = \text{Rabi frequency} \quad (5.4)$$

$$\Omega = 2\omega - \omega_{ba} + 2 \frac{\partial \phi}{\partial t}$$

and describe the evolution of the entire system in the travelling reference frame

$$\eta = \frac{x}{c}, \quad \tau = t - \frac{x}{c}$$

Finally, the coupled Schrödinger-Maxwell equations can be cast into the form

$$\begin{aligned} \frac{\partial R_1}{\partial \tau} &= \left(\frac{\gamma}{\sqrt{1+\gamma^2}} \omega_R + \Omega \right) R_2 + \frac{\omega_R}{\sqrt{1+\gamma^2}} R_3 \\ \frac{\partial R_2}{\partial \tau} &= - \left(\frac{\gamma}{\sqrt{1+\gamma^2}} \omega_R + \Omega \right) R_1 \\ \frac{\partial R_3}{\partial \tau} &= - \frac{\omega_R}{\sqrt{1+\gamma^2}} R_1 \\ \frac{\partial \omega_R}{\partial \eta} &= g \omega_R R_1 - \ell \omega_R \\ \frac{\partial \Omega}{\partial \eta} &= g \left(\frac{\partial R_2}{\partial \tau} - \gamma \frac{\partial R_3}{\partial \tau} \right) \end{aligned} \quad (5.5)$$

The field damping term $-\ell \omega_R$ has been added phenomenologically to describe the effects of diffraction and other non-resonant scattering losses. The coupled equations (5.5) are valid in

the coherent limit, i.e., when atomic relaxation effects can be neglected. In this limit three exact relations can be derived, two in the form of conservation laws, the third providing a link between the field intensity and the detuning variable.

The first relation is a consequence of the probability conservation (Eq. (2.10)) which in terms of the Bloch variables takes the form

$$R_1^2 + R_2^2 + R_3^2 = 1 \quad (5.6)$$

The second, which is valid only for resonant propagation ($\Omega=0$), is a direct consequence of the second and third atomic equations. These can be combined to give

$$R_2 - \gamma R_3 = R_2(0) - \gamma R_3(0) = -\gamma \quad (5.7)$$

The third exact relation follows from the field equations after they have been combined to yield

$$\frac{\partial}{\partial \eta}(\omega_R \Omega) = -\lambda \omega_R \Omega \quad (5.8)$$

Equation (5.8) can be integrated at once with the result

$$(\omega_R \Omega)_\eta = (\omega_R \Omega)_{\eta=0} e^{-\lambda \eta} \quad (5.9)$$

This last result shows that, in the coherent limit, a resonant pulse ($\Omega \neq 0$) can propagate through the active medium always maintaining the resonance condition.

VI. RESONANT COHERENT PROPAGATION. ENERGY EQUATION

The coupled equations (5.5) can be simplified considerably in the case of resonant propagation, where it can be easily shown that the Bloch equations are formally satisfied by^{4(a),8}

$$\begin{aligned} R_1 &= \frac{R_3^e}{\sqrt{1+\gamma^2}} \sin \sigma \\ R_2 &= \frac{R_3^e \gamma}{1+\gamma^2} (\cos \sigma - 1) \\ R_3 &= \frac{R_3^e}{1+\gamma^2} (\cos \sigma + \gamma^2) \quad , \quad (R_3^e = \text{equilibrium population}) \end{aligned} \quad (6.1)$$

provided the variable $\sigma(\eta, \tau)$ is connected to the Rabi frequency by

$$\frac{\partial \sigma}{\partial \tau} = \omega_R \quad (6.2)$$

or by

$$\sigma(\eta, \tau) = \int_0^\tau d\tau' \omega_R(\eta, \tau') \quad (6.3)$$

Thus $\sigma(\eta, \tau)$ is proportional to the accumulated pulse energy up to the local time τ . Clearly the total pulse energy $\Sigma(\eta)$ will be given by

$$\Sigma(\eta) = \lim_{\tau \rightarrow \infty} \sigma(\eta, \tau) \quad (6.4)$$

The dynamics of the coupled atom-field system is governed by Eq. (6.1) and by the partial differential equation

$$\frac{\partial^2 \sigma}{\partial \eta \partial \tau} = \frac{g}{\sqrt{1+\gamma^2}} \sin \sigma \frac{\partial \sigma}{\partial \tau} - \lambda \frac{\partial \sigma}{\partial \tau} \quad (6.5)$$

which follows directly from Eq. (6.2) and the field equations. On the surface, Eq. (6.5) is reminiscent of the so-called area equation first proposed by Arecchi and Bonifacio to describe the pulse evolution in a homogeneously broadened laser amplifier under coherent and resonant propagation conditions². Two main differences will be recognized: first of all, the gain term in the Arecchi-Bonifacio area equation has the form $G \sin \sigma$, where G is a gain parameter; secondly, the "area" σ is not a measurable quantity in the one-photon amplifier theory.

A mathematical consequence of the structure of the gain term in our Eq. (6.5) is that the equation can be integrated exactly with respect to the local time with the result

$$\frac{\partial}{\partial \eta} \Sigma(\eta) = -\lambda \Sigma(\eta) + \frac{g}{\sqrt{1+\gamma^2}} (1 - \cos \Sigma(\eta)) \quad (6.6)$$

The steady state behavior of the total pulse energy, $\Sigma(\eta)$, is governed by the transcendental equation

$$1 - \cos \Sigma(\infty) = \frac{\sqrt{1+\gamma^2}}{g} \lambda \Sigma(\infty) \quad (6.7)$$

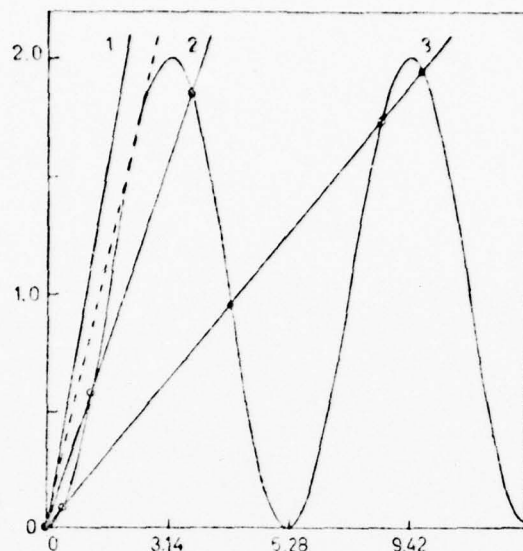


Figure 3. The asymptotic steady state solution of the energy equation (Eq. (6.7)) correspond to the intercepts of the straight line $\sqrt{1+\gamma^2} \frac{L}{R}$ with the curve $1-\cos L$. The straight lines 1, 2 and 3 have slopes equal to 1, 1/2, 1/5 respectively. The stable solutions are marked with solid circles. The unstable solutions are marked with open circles. The critical slope (dashed line) equals 0.7246.

It is clear from Fig. 3 that non-trivial solutions of Eq. (6.7) will exist only if the gain to loss ratio exceeds a certain threshold value and also that, if such threshold is exceeded, multiple steady state solutions are possible. Which of the possible multiple solutions is going to be realized physically, depends on the incident value $L(0)$.

By inspection of Fig. 3 several quantitative conclusions can be drawn:

- 1) Two simultaneous requirements must be satisfied for the asymptotic propagation of a pulse having a total energy $\Sigma(\infty) \neq 0$: the parameter $\sqrt{1+\gamma^2} \frac{L}{R}$ must be smaller than the critical value 0.7246 (the slope of the dashed line in Fig. 3), and the incident pulse energy must exceed

the numerical value corresponding to the first unstable root of Eq. (6.7). If both conditions are satisfied, the total energy will converge to a stable non-vanishing value. The stability of the asymptotic solution of Eq. (6.7) can be assessed at once by analyzing the sign of $dZ/d\eta$ in the vicinity of the roots.

- ii) The output value of the pulse energy can be larger or smaller than the input value $Z(0)$, depending on the magnitude of $Z(0)$ relative to the nearest stable asymptotic root.
- iii) There is no small signal gain, i.e. even if the gain to loss ratio is sufficiently large, an input pulse whose energy is smaller than the first unstable root will not be amplified.

More detailed information on the transient evolution and envelope modulation requires the use of a computer simulation. As we show in the next section, the pulse envelope does not approach a steady state¹¹. Our simulation indicates that, if the threshold conditions are met, the propagating pulse narrows indefinitely as the energy approaches its stable asymptotic value. Furthermore, whenever multiple stable solutions are possible, the n -th stable root $Z(n)$ corresponds to a pulse envelope that has been split into $(n-1)$ distinct pulses.

VII. COMPUTER SIMULATIONS. COHERENT PROPAGATION

The set of equations (5.5) has been analyzed with a hybrid computer. In this section we summarize the main results with an eye on the following features of the problem

- i) Validity of the threshold conditions for propagation of simple and multiple pulses.
- ii) Transient evolution of single and multiple pulses.
- iii) Approach to steady state of the pulse energy.

The system is assumed excited in a swept excitation mode corresponding to the initial and boundary conditions

$$\begin{aligned}
 R_1(\tau=0, \eta) &= R_2(\tau=0, \eta) = 0 \\
 R_3(\tau=0, \eta) &= 1 \\
 \Omega(\tau, \eta=0) &= 0 \\
 \omega_R(\tau, \eta=0) &= \omega_R(\tau)
 \end{aligned}
 \tag{7.1}$$

The input pulse intensity was assigned the shape

$$\omega_R(\tau) = \omega_R^0 \sin^2 (\pi \tau / \tau_p)$$

where τ_p is the pulse duration from the leading to the trailing edge.

As expected, the computer simulation shows that if the detuning variable Ω is zero at the boundary of the medium, it remains equal to zero during the evolution of the pulse.

The threshold conditions have been checked by choosing a gain to loss ratio smaller than the threshold value (reciprocal slope of the dashed line in Fig. 3) or an incident pulse energy smaller than the first unstable root corresponding to a sufficient large gain to loss ratio in Fig. 3. In both cases the incident pulse is attenuated during the propagation.

The first two examples of propagation above threshold are shown in Figs. 4 and 5. These simulations display the evolution of two input pulses with initial energies $\Sigma(0) = 3$ and $\Sigma(0) = 8$, respectively, which propagate in a medium characterized by a gain to loss ratio equal to 2. Under these conditions, Eq. (6.7) and Fig. 3 predict the propagation of a single pulse. This is confirmed in Figs. 4 and 5.

In the case of Fig. 5, the incident pulse has an energy larger than the expected steady state value $\Sigma(\infty)$. Strong transient modulation and energy loss characterize the pulse evolution. Still, as observed with all the simulations where the threshold conditions were satisfied, peak power amplification occurs even when the pulse experiences a net energy loss. An example of pulse break-up is shown in Fig. 6. The gain to loss ratio equals 5 and the input energy is set equal to 9.8. According to Eq. (6.7) and Fig. 3, the asymptotic value of the pulse energy is predicted to correspond to the third stable solution ($\Sigma(\infty) = 0$ is considered to be the first stable root). Two propagating pulses are observed under these conditions. By contrast (Fig. 7), a pulse with a smaller input energy ($\Sigma(0) = 5$) travelling in a medium with the same gain to loss ratio does not exhibit pulse break-up. The predicted asymptotic value of the pulse energy equals the second stable root displayed in Fig. 3 for this value of $g/2\sqrt{1+\gamma^2}$.

In all the cases shown above, the total pulse energy at every section along the amplifier was read off at the far right of the solid lines representing the evolution of $\sigma(\tau, \eta)$. With due allowance for the fact that some of the simulations had to be terminated before reaching their asymptotic stage, the agreement with the predicted values of $\Sigma(\infty)$ was found to be quite satisfactory.

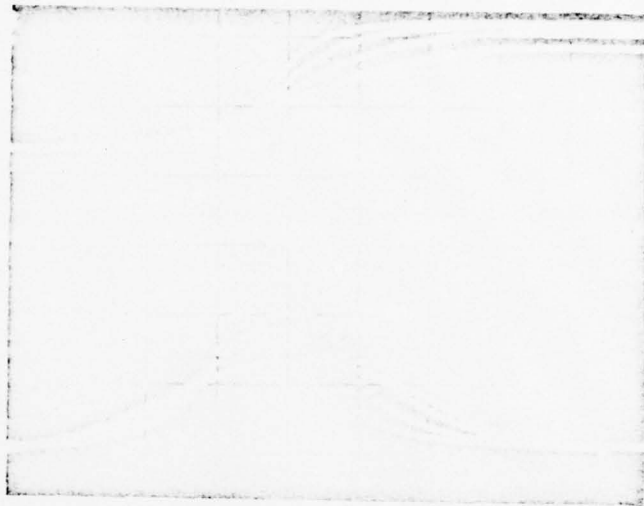


Figure 4. Computer simulation illustrating the evolution of the pulse intensity through the amplifying medium. The different dashed curves represent the intensity envelope in different sections of the amplifier. The solid curves are the corresponding integrated energies $\sigma(\eta, \tau)$. The value of $\sigma(\eta, \tau)$ at the far right gives the total energy $Z(\eta)$. The horizontal axis is the local time axis, with $\tau=0$ (leading edge of the pulse) at the far left. The input energy is $Z(0)=3$ and the gain to loss ratio $g/l \sqrt{1+\gamma^2}$ equals 2.



Figure 5. Evolution of a pulse with an initial energy $I(0)=8$; the gain to loss ratio equals 2 as in Fig. 4. Note the transient envelope modulation and pulse energy loss.



Figure 6. Evolution of a pulse with initial energy $L(0)=9.8$ in a medium with a gain to loss ratio equal to 5. The asymptotic pulse energy is expected to take a value equal to the third stable root shown in Fig. 3 (straight line #3). Under these conditions, pulse break-up is observed.



Figure 7. Propagation of a pulse with initial energy $E(0)=5$. The gain to loss ratio is the same as in Fig. 6. A single peak is expected on the basis of Eq. (6.7) and Fig. 3.

REFERENCES

- (1) For a nice survey see for example, L. Allen and J.H. Eberly, *Optical Resonance and Two-level Atoms*, John Wiley and Sons (New York), 1976.
- (2) A very extensive literature is available on two-photon processes. For a critical comparison of different theoretical approaches and additional references see for example: D. Grischkowski, in *Laser Applications to Optics and Spectroscopy*, Vol. II of *Physics of Quantum Electronics*, Eds. S.F. Jacobs, M. Sargent III, J.F. Scott, M.O. Scully (Addison-Wesley 1975), D. Grischkowski, M.M.T. Loy, P.F. Liao, *Phys. Rev. A* **12**, 2514 (1975).
- (3) F. Biraben, B. Cagnac, G. Grynberg, *Phys. Rev. Lett.* **32**, 643 (1974),
M.D. Levenson, N. Bloembergen, *Phys. Rev. Lett.* **32**, 645 (1974).

- (4)(a) E.M. Belenov, I.A. Poluektov, Sov. Phys. JETP 29, 754 (1969).
M. Takatsuji, Physica 51, 265 (1971); Phys. Rev. B2, 340 (1970).
N. Tan-no, K. Yokoto, H. Inaba, Phys. Rev. Lett. 29, 1211 (1972).
- (5) M. Takatsuji, Phys. Rev. A11, 619 (1975).
F.H.M. Faisal, J. Phys. B., 10, 2093 (1977).
J.C. Diels, Opt. Quant. Electron 8 513 (1976).
H.P. Yuen, F.Y.F. Chu, Proceedings of the Fourth Rochester Conference on Coherence and Quantum Optics, Eds. L. Mandel and E. Wolf (to be published).
- (6) R.L. Carman, Phys. Rev. A12, 1048 (1975).
- (7) N. Tan-no, K. Yokoto, H. Inaba, J. Phys. B8, 339 (1975);
ibid. B8, 349 (1975).
- (8) L.E. Estes, L.M. Narducci, B. Shamma, Lettere al Nuovo Cimento, Serie 2, 1 175 (1971).
- (9) This logical scheme has a venerable history in laser physics. It was implemented in the context of the one-photon laser amplifier problem by A.T. Arecchi, R. Bonifacio IEEE, Jour. Quant. Electron, QE1, 169 (1965).
- (10) See D. Grischkowski et al. in Ref. 2.
- (11) This result was shown analytically by H.P. Yuen and F.Y.F. Chu in Ref. 5.

3. The selection of an active medium

On the basis of the theoretical analysis of Section 2, an appropriate atomic system should be able to support a population inversion between two levels of the same parity. These two levels should be connected by a sufficiently large non-linear susceptibility, but at the same time the depletion of the upper state by natural relation to lower lying states should be kept reasonably low. These requirements appear difficult to satisfy simultaneously because, while on the one hand the third order susceptibility can be enhanced significantly by the presence of $\frac{a}{\Lambda}$ near resonant intermediate level, the radiative decay rate from the upper state is also increased considerably by the presence of lower lying allowed transitions.

One must also keep in mind that both the pump and the incident pulse should be tunable and that the power level of the incident pulse should be fairly large to overcome the threshold requirements for two photon amplification. Thus the choice of an active system should be made while keeping in mind the availability of tunable sources for the pumping and the amplification stages of the process.

A reasonable compromise appears to be offered by atomic Calcium whose lowest lying singlet energy levels are shown in Fig.1 of Ref.9 (See enclosed reprint). We have directed our efforts to producing a population inversion between the 1D_2 level at 21850 cm^{-1} and the 1S_0 ground state. After completion of the pumping process an infrared pulse of tunable laser radiation would stimulate two-photon decay of the atoms and amplification at the same frequency as the incident field.

Inversion between the 1D_2 level and the ground state can be achieved in practice only with the help of a higher lying level (Coherent two-photon absorption between the 1S_0 and the 1D_2 levels could conceivably be used as well, but the practical realization of this scheme looks very difficult at this time).

We have decided to pump the upper level by way of the 4P_1 level at 36732 cm^{-1} . This level is coupled to the ground state by a dipole allowed transition which requires the absorption of ultraviolet radiation of 2721.65 Å^0 . The branching ratios favor the decay of the excited 4P_1 state to the 4D_2 level so that, at least theoretically, a moderately intense UV pulse of resonant radiation should be able to produce sufficient population inversion between the two levels of interest.

Two-photon amplification should then be possible by sending a pulse of infrared radiation of 9153 Å^0 (the frequency corresponding to 9153 Å^0 is one half of the frequency separation between the 4D_2 level and the ground state).

Both the ultraviolet and infrared sources should be tunable. A practical way to produce an ultraviolet pulse of pump power is to convert the output of a Coumarin dye laser by second harmonic generation with an angle tuned KDP crystal. The infrared pulse can be produced with an IR-125 dye laser excited by a Q-Switched Ruby laser pulse.

The practical realization of this scheme has proven to be a considerable challenge which has delayed our progress more than anticipated. At this time, however we feel that the remaining difficulties can be overcome. A survey of our progress along these lines and an appraisal of our present chances for implementing this scheme will be discussed further on in this report.

4. Preparation of the active medium

In order to estimate the pump requirements we consider the simplified energy level diagram shown in Fig.4.1

The correspondence between the levels shown in the figure and the Calcium levels of interest is listed in Table (4-1). We ignore collision induced relaxation processes out of the singlet manifold into the lower lying triplet states because these are expected to be unimportant in the pressure range of the experiments. Let the total number of atoms in the three levels be N with

$$N = n_1 + n_2 + n_3$$

The population rate equation are

$$\frac{dn_1}{dt} = (A_{21} + \rho_p B_{21}) n_2 - \rho_p B_{12} n_1$$

$$\frac{dn_2}{dt} = -(A_{23} + A_{21} + \rho_p B_{21}) n_2 + \rho_p B_{12} n_1$$

$$\frac{dn_3}{dt} = A_{23} n_2$$

Where the coefficients A_{ij} and B_{ij} are the usual Einstein's A and B coefficients with A_{ij} measured in sec^{-1} and B_{ij} in $\frac{\text{cm}^3}{\text{erg sec}^2}$. The parameter ρ_p is the pump energy density per unit bandwidth ($\frac{\text{erg sec}}{\text{cm}^3}$). For the chosen levels of Calcium, the parameters are listed in Table (4-2).

We are concerned with the evolution of the population of level 3. This can be obtained from the rate equations after some elementary calculations. The result is

$$n_3(t) = N \left[\frac{c}{c-b} (1 - e^{-bt}) - \frac{b}{c-b} (1 - e^{-ct}) \right]$$

where

$$b = \frac{k_2 + k_3 - ((k_2 + k_3)^2 - 4k_3k_4)^{1/2}}{2}$$

$$c = \frac{k_2 + k_3 + ((k_2 + k_3)^2 - 4k_3k_4)^{1/2}}{2}$$

and

$$k_2 = A_{23} + A_{21} + \rho_P B_{21}$$

$$k_3 = \rho_P B_{12} ; \quad k_4 = A_{23}$$

If we assume an ultraviolet pump pulse of about 100 KW, duration 600 sec., and cross section 1 cm^2 , the energy density of the pump is of the order of 30 erg/cm^3 . If in addition the bandwidth of the pump is 1 \AA , the corresponding energy density per unit bandwidth becomes

$$\rho_P \approx 1.5 \times 10^{-11} \frac{\text{erg}}{\text{cm}^3} \text{ sec}$$

With these estimates, the appropriate transition rates and the time dependent population of the third level take on the values listed in Table (4-3).

Although relaxation processes out of the level 3 will partially deplete the inversion, the estimate obtained without consideration of such decay mechanisms is expected to be reasonable under the conditions of our experiments.

T A B L E 4 - 1

Energy Level	Spectroscopic Classification	Energy (cm^{-1})
1	$4s^2 \ ^1S_0$	0
2	$3d4p \ ^1P_1$	36732
3	$4s3d \ ^1D_2$	21850

$$\lambda_{21} = 2721.65 \text{ \AA}^{\circ}$$

$$\lambda_{23} = 6717.69 \text{ \AA}^{\circ}$$

$$\lambda_{31} = 9153\frac{1}{2} \text{ \AA}^{\circ}$$

TABLE 4 - 2

$$A_{21} = 2.7 \times 10^5 \text{ sec}^{-1}$$

$$A_{23} = 1.2 \times 10^7 \text{ sec}^{-1}$$

$$B_{21} = 6.01 \lambda^3 A_{21} \frac{\text{cm}^3}{\text{erg sec}^2}, \quad (\lambda \text{ measured in } \text{\AA})$$

$$B_{12} = 6.01 \lambda^3 \frac{g_2}{g_1} A_{21}$$

$$g_2 = 3, \quad g_1 = 1$$

$$B_{21} = 3.27 \times 10^{16} \frac{\text{cm}^3}{\text{erg sec}^2}$$

$$B_{12} = 9.81 \times 10^{16} \frac{\text{cm}^3}{\text{erg sec}^2}$$

TABLE 4 - 3

$$k_1 = A_{21} + \rho_p B_{21} = 2.7 \times 10^6 \text{ sec}^{-1}$$

$$k_2 = A_{23} + k_1 = 1.5 \times 10^7 \text{ sec}^{-1}$$

$$k_3 = \rho_p B_{12} = 7.4 \times 10^6 \text{ sec}^{-1}$$

$$k_4 = A_{23} = 1.2 \times 10^7 \text{ sec}^{-1}$$

t (nsec)	$\frac{n_3 - n_1}{N}$
50	- 0.63
100	- 0.29
200	0.22
300	0.54
400	0.73

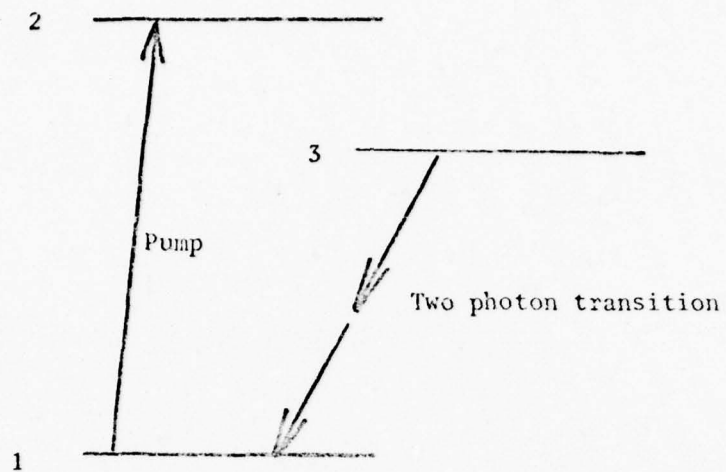


FIG. 4-1

SCHEMATIC ENERGY LEVEL DIAGRAM
OF THE ACTIVE MEDIUM

5. Monitoring the Calcium Cell

A well known problem in atomic spectroscopy is posed by the necessity for measuring the density of atoms in a gaseous phase. Light absorption techniques have been developed over the years whenever vapor pressure curves have been found not sufficiently accurate for this purpose. In our case, for example, the vapor pressure data for Calcium which are reported by CRC Handbook of Chemistry and Physics cover the temperature range 926°C - 2290°C. Our measurements are carried out around 800°C, (below the Ca melting point); consequently, the available data are of no use for our needs.

If one knows the oscillator strength of a particular allowed transition, a measurement of the atomic density can be carried out, in principle, by recording the attenuation of a light beam in the neighborhood of the absorption line. One of the absorption lines of Calcium atoms ($1S_0 \rightarrow 4P_1$ at 4226.73 Å) is especially suited for this purpose because of its large oscillator strength. However, while it is correct to argue that the attenuation coefficient can yield the atomic density directly, the practical extraction of this information from the data is not trivial for the reasons explained below.

Consider a column of gas of length ℓ and let $I_{in}^{true}(\nu)$ be the incident flux per unit frequency range. In the limit where Beer's law holds the transmitted flux per unit frequency range is

$$I_{out}^{true}(\nu) = I_{in}^{true}(\nu) e^{-k(\nu)\ell}$$

where $k(\nu)$, the true absorption coefficient per unit length, is proportional to the atomic density (strictly speaking $k(\nu)$ is proportional to the ground state atomic population; however, in most instances, the excited

population is entirely negligible). If the dispersing instrument used to resolve the absorption profile had infinite resolution, the measurement of $k(\nu)$ would be completely trivial.

In reality, of course, a spectrometer is a linear optical instrument with a transfer function of finite width. Let $G(\nu)$ be the spectrometer response to an infinitely narrow atomic line of unit strength. The linearity of the instrument insures that the response to a collection of narrow lines of strengths A_1, A_2, \dots, A_n will be such that the observed spectrum takes the form

$$I^{obs} = \sum_k A_k G(\nu - \nu_k)$$

If the spectrum to be analyzed has a continuous profile $I^{true}(\nu)$, the observed spectrum has the form

$$I^{obs}(\nu) = \int_{-\infty}^{+\infty} d\nu' I^{true}(\nu') G(\nu - \nu')$$

In particular, if the light entering the spectrometer is emerging from a column of absorbing gas, the observed and the incident spectrum will be related by the convolution integral

$$I_{out}^{obs}(\nu) = \int_{-\infty}^{+\infty} d\nu' I_{in}^{true}(\nu') e^{-k(\nu')\ell} G(\nu - \nu')$$

It is clear that even if the empirical relation

$$I_{out}^{obs}(\nu) = e^{-k^{obs}(\nu)\ell} I_{in}^{obs}(\nu)$$

should hold between the observed spectral distributions, no simple relation is expected to exist between $k^{\text{obs}}(\nu)$ and the true absorption coefficient $k(\nu)$. It is also clear that the observed line will bear little resemblance to the true absorption line in general.

In principle, one would think that the elimination of the instrumental broadening could be carried out by deconvolution techniques. In fact, given

$$I_{\text{out}}^{\text{obs}}(\nu) = \int d\nu' I_{\text{out}}^{\text{true}}(\nu') G(\nu - \nu')$$

the Fourier transform of the convolution integral leads to

$$\tilde{I}_{\text{out}}^{\text{obs}}(t) = \tilde{I}_{\text{out}}^{\text{true}}(t) \tilde{G}(t)$$

and

$$\tilde{I}_{\text{out}}^{\text{true}}(t) = \tilde{I}_{\text{out}}^{\text{obs}}(t) / \tilde{G}(t)$$

Hence the inverse Fourier transform

$$I_{\text{out}}^{\text{true}}(\nu) = \mathcal{F}^{-1} \left[\tilde{I}_{\text{out}}^{\text{obs}}(t) / \tilde{G}(t) \right]$$

gives the spectral profile. This procedure works well for noise free data. However, almost any amount of noise will make the numerical inversion hopeless, even if one could measure the instrument function G with good accuracy.

Accurate (10-20%) information on the atomic density can still be derived experimentally even with an imperfect spectrometer: this, however, requires knowledge of the atomic lineshape. On the contrary, no detailed knowledge of

the instrument function is needed.

There are five basically distinct line broadening mechanisms:

1. Natural broadening. The natural lineshape has a Lorentzian profile with a half-width given by

$$\Delta \nu_N = \frac{1}{2\pi\tau} \equiv \frac{A_{21}}{2\pi}$$

where τ is the natural decay time of the transition and A_{21} is the Einstein A-coefficient.

2. Doppler broadening. The Doppler line has a Gaussian shape with a half-width given by

$$\Delta \nu_D = \frac{2\sqrt{\ln 2}}{\lambda_0} \sqrt{\frac{2kT}{M}}$$

where λ_0 is the transition wavelength and M is the mass of the atom.

3. Holtzmark broadening. This line broadening mechanism is due to collisions between atoms of the same kind. In many instances, this effect is negligible below 10^{-2} Torr.

4. Lorentz broadening. This line broadening mechanism is due to collisions between the atoms of interest and the buffer gas. This effect is small, below 5 Torr of foreign gas.

5. Stark broadening. This is due to electrostatic and Van der Waals interactions. This is negligible when 3 and 4 are negligible in our experimental situation.

It is easy to calculate the lineshape due to the combined natural plus Doppler broadening. The result is

$$k(\nu) = k_0 \frac{a}{\pi} \int_{-\infty}^{+\infty} \frac{e^{-y^2} dy}{a^2 + (\omega_r - y)^2}$$

$$a = \frac{\Delta \nu_N}{\Delta \nu_D} \sqrt{\ln 2}$$

$$\omega_\nu = \frac{2(\nu - \nu_0) \sqrt{\ln 2}}{\Delta \nu_D}$$

$$k_0 = \frac{\lambda_0^3}{8\pi} \frac{g_2}{g_1} \frac{N A_{21}}{\sqrt{\frac{2\pi kT}{M}}}$$

where g_2 and g_1 are the degeneracy factors of the excited and ground state levels and N is the number density of atoms per unit volume. The parameter α represents the ratio of the natural to Doppler linewidths, while ω_ν is the frequency of the line measured from line center in units of Doppler widths. The physical meaning of k_0 follows from the evaluation of $k(\nu)$ at line center ($\omega_\nu = 0$).

In fact,

$$k(\nu = \nu_0) = k_0 (1 - \text{Erf}(\alpha)) e^{\alpha^2};$$

a typical value of α for an atomic gas is $\approx 10^{-2}$ so that

$$k(\nu = \nu_0) \approx k_0.$$

It would be a mistake to assume that because of the smallness of α one can ignore the natural broadening, because the wings of the absorption curve can be dominated by natural rather than Doppler absorption, especially for sufficiently

large atomic densities. Hence for accurate work the lineshape $k(\nu)$ given by the above integral representation will be used.

For small values of α an excellent approximation to the lineshape is given by

$$k(\omega_r) = k_0 \left[e^{-\omega_r^2} - \frac{2\alpha}{\sqrt{\pi}} (1 - 2\omega_r F(\omega_r)) \right]$$

where $F(\omega_r)$ is the Dawson integral

$$F(\omega_r) = e^{-\omega_r^2} \int_0^{\omega_r} e^{x^2} dx.$$

Our previous comments on the importance of retaining at least the lowest order dependence of $k(\omega_r)$ on α are well justified. If $k(\omega_r)$ were simply given by $k_0 e^{-\omega_r^2}$, its value would be practically zero after 4 or 5 Doppler widths, whereas this is not the case if the first order correction is retained. Our numerical analysis shows clearly that if one neglects the α -dependence in the absorption lineshape, the resulting atomic density can be in error by large amounts.

The structure of the Dawson integral suggests that numerical errors are likely to become very severe for large values of ω_r . (In practice we found that values as large as 30 are required for a sufficiently accurate evaluation of the curve of growth.) For values of ω_r of the order of or greater than 6, the following asymptotic approximation was found to be very accurate

$$1 - 2\omega_r F(\omega_r) \simeq - \left(\frac{1}{2\omega_r^2} + \frac{3 \cdot 1}{(2\omega_r^2)^2} + \frac{5 \cdot 3 \cdot 1}{(2\omega_r^2)^3} + \dots \right)$$

Note, however that the above is an asymptotic series and that its accuracy is not only a function of the number of terms which are retained but also of

the magnitude of ω_v . For $\omega_v > 6$, the four term expansion was found to be very accurate (a few parts per million).

Now that the atomic lineshape is known, we are in a position to relate the observed absorption curve to the atomic population density. Given

$$I_{out}^{obs}(\nu) = \int_{-\infty}^{+\infty} d\nu' I_{in}^{true}(\nu') e^{-k(\nu')\ell} G(\nu-\nu')$$

we integrate the left and right hand sides with respect of ν over a sufficiently large range to include all the required spectral features. The shape of the observed spectrum shows clearly that the ν integral cannot be extended over the entire frequency axis, otherwise the result of the integration will diverge. It will be only necessary to extend the range of integration until the integral

$$\int d\nu G(\nu-\nu')$$

becomes independent of ν' . Strictly speaking this implies, in turn, that the ν' integration must also be carried out over a finite range. In practice, there is no problem with these restrictions owing to the very narrow region of the frequency axis where the relevant spectral information is contained.

With this in mind we obtain

$$\int d\nu I_{out}^{obs}(\nu) = \alpha \int d\nu' I_{in}^{true}(\nu') e^{-k(\nu')\ell}$$

where α is a constant defined by

$$\alpha = \int d\nu G(\nu-\nu')$$

If, in addition, the incident flux has a white spectrum in the region of interest, we have

$$\int d\nu I_{out}^{obs}(\nu) = \alpha I_{in}^{true} \int d\nu' e^{-k(\nu')\ell}$$

The observed signal has the typical shape shown in Fig (5-1). Hence, it follows that

$$\int I_{out}^{obs}(\nu) d\nu = \int_{\Delta\nu} I_{in}^{obs} d\nu - \int_{\Delta\nu} f(\nu) d\nu$$

where $f(\nu)$ is the absorption signal of interest. Its area

$$\int_{\Delta\nu} f(\nu) d\nu$$

is shaded in the figure.

If we now define as the equivalent width, the parameter w_ν such that

$$\int_{\Delta\nu} f(\nu) d\nu = w_\nu I_{in}^{obs},$$

we finally arrive at

$$w_\nu = \int d\nu (1 - e^{-k(\nu)\ell})$$

In practice w_ν can be arrived at by graphical integration of the signal $f(\nu)$, or by other more empirical techniques. (Because of the arbitrary units we found it convenient to cut the observed absorption lines and to weigh them on a precision balance. The ratio of the measured weight to the weight of a unit area gives a reasonable first approximation to the required area). If $f(\nu)$ has a highly symmetric shape, a reasonable approximation for w_ν will be given by the relation

$$w_\nu = W_\nu' f_{max} / I_{in}^{obs}$$

where W_ν' is the full width at half height of $f(\nu)$. (See Fig (5-2)). In general, a spectrometer will produce an absorption spectrum as a function of wavelength. The equivalent width w_λ in wavelength space is related to the absorption

coefficient $k(\omega_v)$ by

$$W_\lambda = \sqrt{\frac{2\pi kT}{M}} \frac{2\lambda}{c\sqrt{\pi}} \int_0^\infty d\omega_v (1 - e^{-k(\omega_v)l})$$

where ω_v is the usual dimensionless frequency measured from line center in units of the Doppler width.

A typical experiment can be carried out with a tungsten-halogen lamp (500W) whose output is collimated through the Ca cell. We found it more convenient to bring the sample at a high temperature first and to collect the temperature dependent data by cooling off the oven in suitable steps ($\Delta T \approx -25^\circ\text{C}$). This method has the advantage that the effects of the oxide layer, which, almost unavoidably, coats the sample even after careful handling, are minimized. Heating up the sample from room temperature was observed to lead to irregular increases in the vapor pressure and to sudden changes of absorption which we attribute to the removal of the oxide layer at a sufficiently high temperature.

By varying the temperature, different values of the equivalent width are measured from the absorption spectra. The data reduction proceeds as follows. For a fixed value of T , a set of theoretical values of W_λ are constructed from the theoretical expression as a function of $\ln(Nl)$ where l is the unknown length of the gas column. The required value of $\ln(Nl)$ is found as shown below in Fig. 5-3. The set of experimental values of W_λ plotted as a function of the interpolated values of $\ln(Nl)$ will provide the required curve of growth. (See fig (5-4)).

In principle the method outlined above is capable of removing the effects of the finite instrument transfer function. However, it is always good practice

to operate the spectrometer in such a way as to introduce the least amount of instrumental broadening. After selecting the proper grating and blaze angle, one should operate in the diffraction order that produces the largest throughput for fixed entrance and exit slit widths. In our case, with a $600 \text{ } \frac{\text{L}}{\text{mm}}$ grating and blaze angle for $1 \mu\text{m}$, we found that the optimum operating diffraction order for highest throughput was the second. We decided to carry out absorption measurements in third order because the loss of output signal was not severe enough to offset the increased resolution from second to third diffraction order.

The choice of the slit widths is the next step. We found that with input and output slits set at $5 \mu\text{m}$, the output signal was still adequate enough to allow an essentially noise free scan of the absorption line. The choice of narrow slits enables us to reduce the amount of background signal and to enhance substantially the ratio of peak absorption to maximum output intensity, even at low temperatures.

It is observed, in addition, that for decreasing temperatures, the absorption profile looks more and more triangular in shape. This is due to the reduced width of the absorption line and to the effect of the convolution of the temperature independent instrumental profile with the narrow atomic line. (See Fig. 5-5, 5-6, 5-7).

It is especially in this temperature range that the equivalent width method becomes useful because direct information about the absorption process is buried completely under the instrumental transfer function.

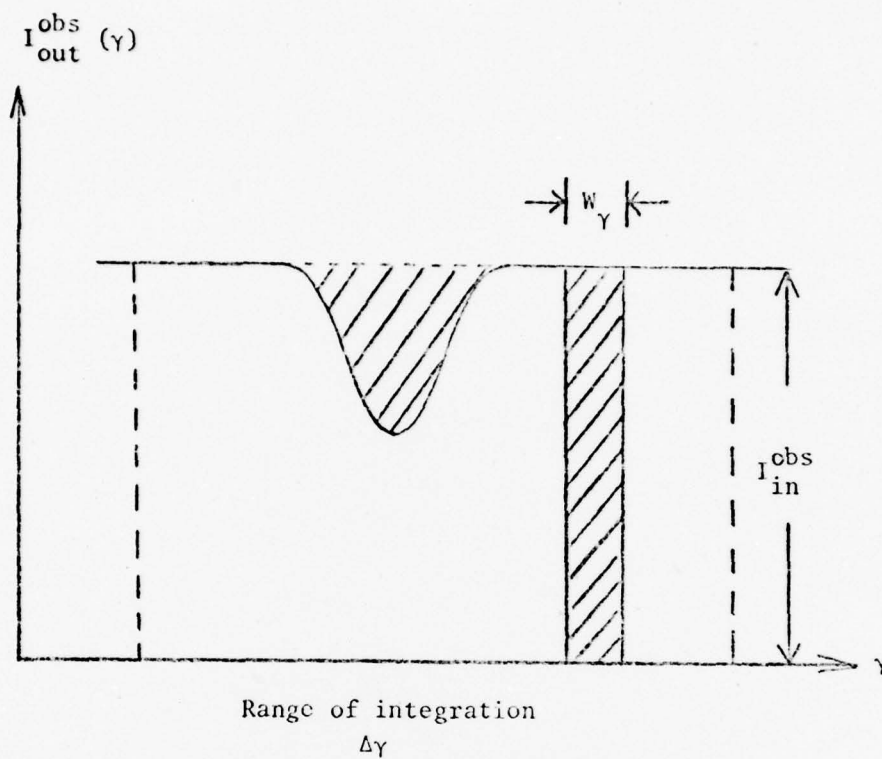


FIG. 5-1

ABSORPTION SPECTRUM OF A SIMPLE ATOMIC LINE.
 THE RECTANGLE OF WIDTH w_γ HAS THE SAME AREA
 AS THE SHADED PORTION OF THE ABSORPTION LINE.

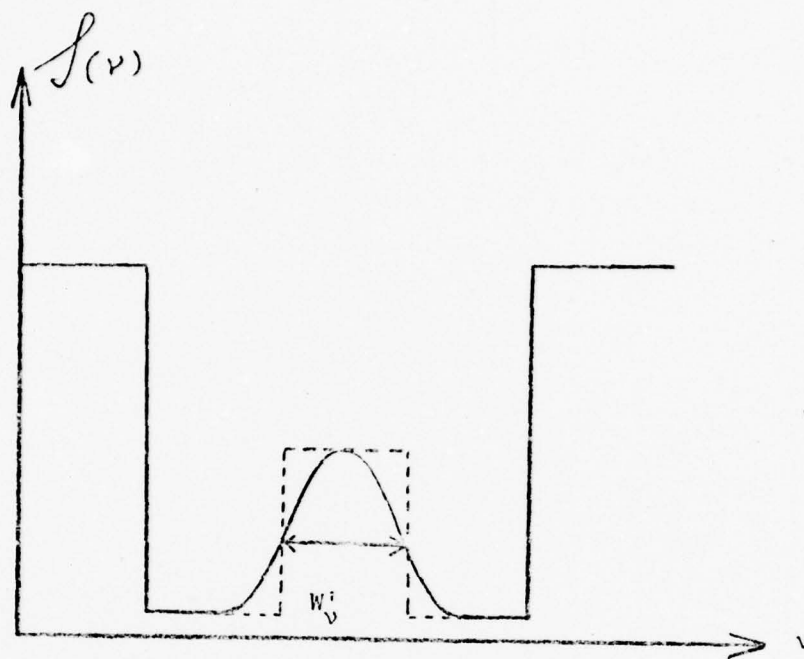


FIG. 5-2

A ROUGH APPROXIMATION FOR THE EQUIVALENT WIDTH w_v^i CAN BE OBTAINED AS SHOWN IF THE ABSORPTION LINE IS SYMMETRIC.

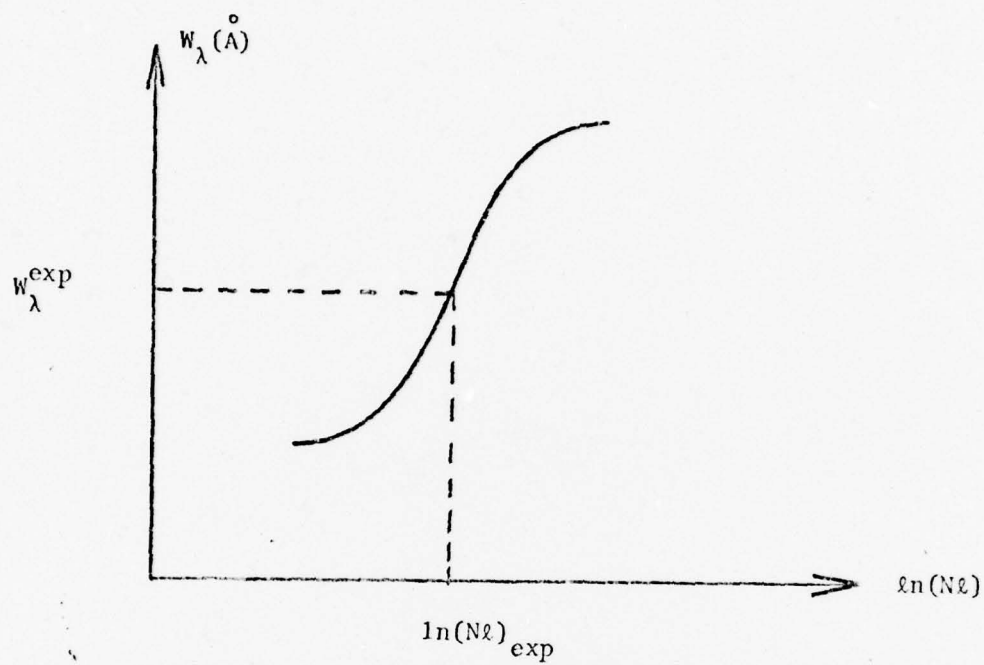


FIG. 5-3

THEORETICAL CURVE OF GROWTH FOR A FIXED VALUE OF THE TEMPERATURE. THE ATOMIC DENSITY CAN BE FORMED AS THE ABSCISSA OF THE CURVE OF GROWTH CORRESPONDING TO THE EXPERIMENTAL EQUIVALENT WIDTH w_{λ}^{exp} .

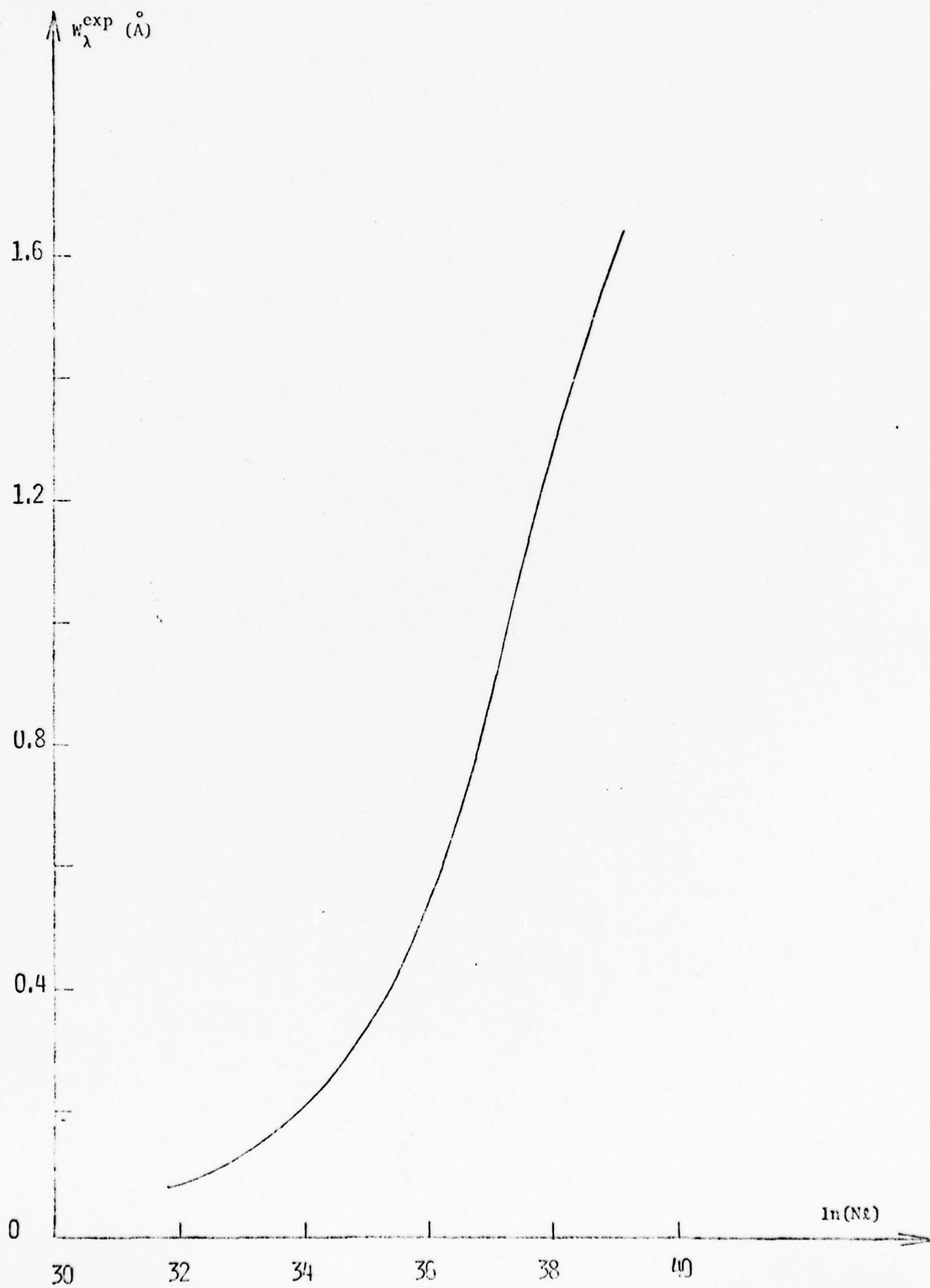
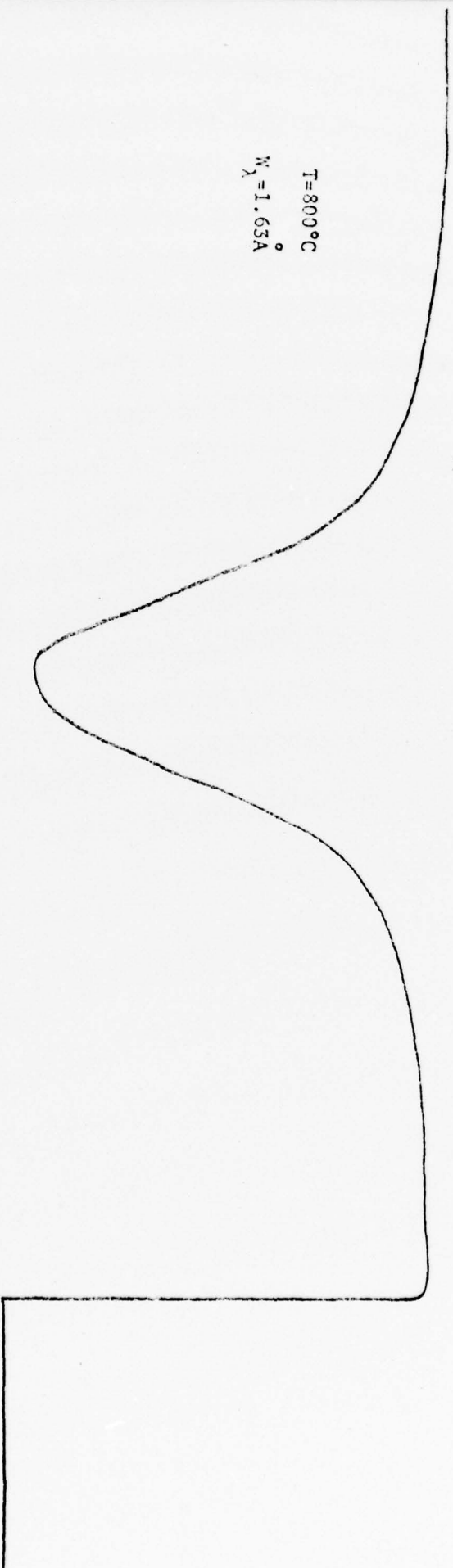


FIG. 5-4

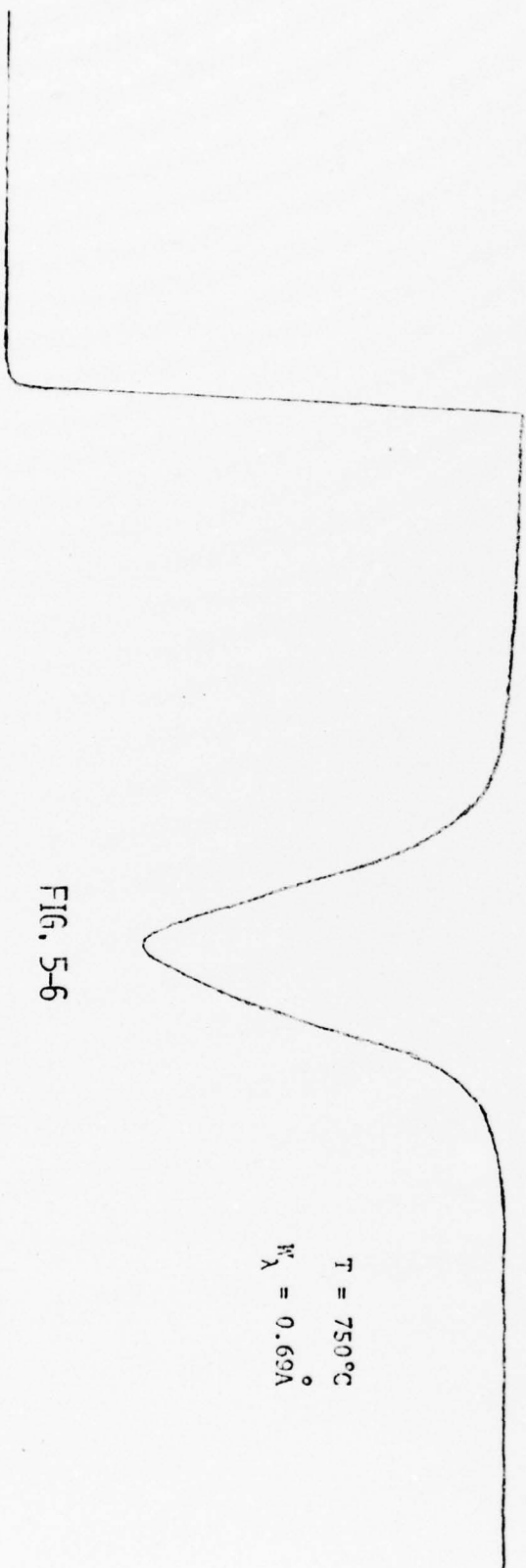
THE EXPERIMENTAL CURVE OF GROWTH CAN BE TRACED BY INTERPOLATING THE EXPERIMENTAL VALUES OF THE EQUIVALENT WIDTH w_{λ}^{exp} AND THE CORRESPONDING VALUES OF $\ln (n_2)$. AN UNKNOWN DENSITY CAN BE DETERMINED BY MEASURING w_{λ}^{exp} AND FINDING THE APPROPRIATE ABSCISSA FROM THE ABOVE CURVE OF GROWTH.



$T = 800^{\circ}\text{C}$
 $w_{\lambda} = 1.63 \text{ \AA}$

FIG. 5-5

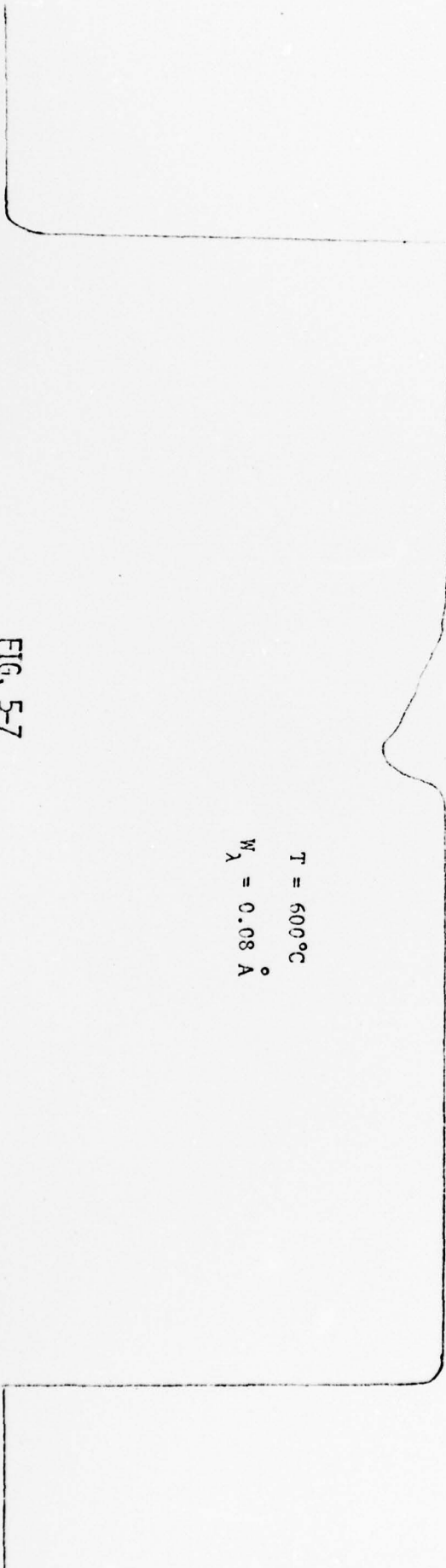
EXPERIMENTAL 4226 \AA ABSORPTION LINE OF Ca. ; w_{λ} IS THE APPROPRIATE EQUIVALENT WIDTH.



$T = 750^{\circ}\text{C}$
 $W_{\lambda} = 0.69\text{\AA}$

FIG. 5-6

EXPERIMENTAL 4226\AA ABSORPTION LINE OF Ca , W_{λ} IS THE APPROPRIATE
EQUIVALENT WIDTH.



$T = 600^{\circ}\text{C}$
 $w_{\lambda} = 0.08 \text{ \AA}$

FIG. 5-7

EXPERIMENTAL 4726 \AA ABSORPTION LINE OF Ca. ; w_{λ} IS THE APPROPRIATE EQUIVALENT WIDTH.

6. Operation of the COU 540A Dye Laser and Second Harmonic Generation

Coumarin 540A, when dissolved in ethanol, has a lasing bandwidth from 517 to 576 nm. However, the dye is extremely susceptible to contamination and great care must be taken during preparation and filling to insure its integrity.

We prepare COU 540A in 1.5 liter quantities according to the following prescription:

The number of grams of powdered dye required to produce a solution of particular concentration is given by the relation

$$\# \text{ gr.} = (M) (M.W.) (L) ,$$

where

gr. = number of grams of powdered dye ,

M = required molarity ,

M.W. = molecular weight of the dye

$$= 309.3 \text{ g/mol}$$

and L = number of liters of solvent (Ethanol).

Accordingly, 1.5 liters of COU 540A lasing solution, at 1×10^{-4} Molar, requires 46.4 grams of powdered dye.

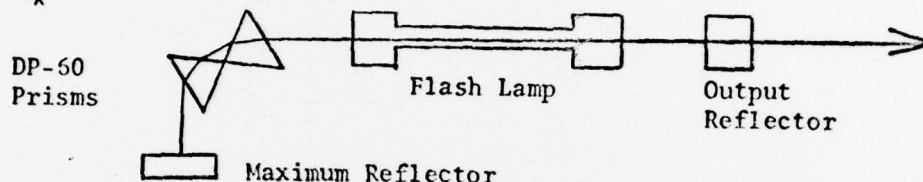
To insure cleanliness during the mixing process, all glassware and accessories are thoroughly washed with 200 proof ethanol prior to mixing. In addition, the dye laser is equipped with an " in line " filtration system to remove any dye crystals or foreign substances that may be present in the circulation system.

While the dye is being mixed, the initial alignment of the dye laser optics is performed.

Since the laser uses a Phase-R DP-60 Prism Assembly as a tuning element,

conventional alignment procedures using a He Ne laser are time consuming and impractical. We developed a quick but accurate technique to visually align the flashlamp-pumped dye laser.

With pure ethanol circulating through the laser firing head, the maximum and output reflectors are visually brought into alignment in a plane-parallel-mirror configuration (PPMC).



This is done as follows.

- 1) With the capacitor bank voltage at zero volts, and the dye circulation system containing pure ethanol (no lasing solution or reflectors), one may orient his eye in such a position as to see coaxially through the center of the flashlamp with both input and output ports appearing concentric.
- 2) One installs the maximum reflector in the PPM configuration and adjusts the horizontal and vertical vernier controls on the maximum reflector mount so that the return image of the eye from the reflector is concentric with the input and output ports of the flashlamp.
- 3) One, then installs the output reflector in the PPM configuration and again adjusts the horizontal and vertical vernier controls on the output reflector mount so that the return image of the eye from the output reflector overlaps the image from the maximum reflector. When this is done, the laser optics is aligned in the plane-parallel mirror configuration. It should be noted that this alignment procedure is relatively accurate, can be performed in a very short time, and does not require the use of a He-Ne laser.

The ethanol, being used in the dye circulation system as a cleaning

solvent, is drained and the freshly mixed COU 540A lasing solution is filled. The dye is allowed to circulate for several minutes to insure that the "in line" filtration system will remove any undissolved dye crystal, or foreign particles that may be present.

The laser system can now be operated in the "broadband" lasing mode. While the system does not yet contain the Phase-R DP-60 dispersive prism assembly, the broadband configuration will allow one to check the thermal stability of the lasing solution in the flashlamp along with the dye concentration and integrity.

Once lasing has been achieved in the broadband mode, the maximum reflector is removed to allow installation of the DP-60 prism assembly. (Fig. 6-1)

The assembly is oriented so that the normal of the input face of prism #1 makes an angle of approximately 60° with the optical axis of the flashlamp.

The capacitor bank is now charged to approximately 10-11 KV. While this voltage value is large enough to permit the spark gap to break down allowing the flashlamp to fire, it is below the lasing threshold of the dye, and consequently, no laser action will be produced. However, by placing a small card several inches from the output face of prism #2 while firing, the fluorescence from the flashlamp emerging from the output of the prism assembly can be readily observed.

When the exact location of this fluorescence has been carefully noted and the capacitor bank voltage reduced to zero volts, an extension rail holding the maximum reflector can be temporarily installed at the output face of prism #2. The maximum reflector should be handled carefully to insure that the horizontal and vertical vernier settings on the reflector mount are not changed from their PPM configuration settings. Under operating conditions, the angle between the output reflector extension rail and the output face of prism #2 will control the

gross frequency tuning of the laser. Fine variation of the output frequency is accomplished by varying the horizontal vernier of the maximum reflector after the extension rail has been positioned and secured.

Optimization of the energy output at the selected frequency will require, at most, fine tuning of the vertical vernier on the maximum reflector mount. The output reflector, still set in the plane parallel mirror configuration, requires no additional optimization.

It should again be noted that this entire alignment can generally be accomplished in less than five minutes and does not require the use of a He Ne laser.

The extended cavity length in the tuning configuration produces a well collimated beam capable of producing burn patterns on Polaroid film at distances up to 6 feet from the output reflector.

The energy of the laser pulse was measured 2 feet from the output reflector using a thermopile (Keithley 149-Milli-Microvoltmeter and a Model No. 108 detector head) calibrated at 50.2 $\mu\text{V}/\text{joule}$. Typical output energies of the order of several tenths of a joule are obtained routinely. For pulse shape studies the beam was monitored by a photodiode (Fig. 6-1) and a Tektronics 7613. A typical pulse has a full width at half maximum of 600 ns. With a pulse energy of 0.2 Joules and a pulse duration of 600 ns, the pulse power of the laser is about 300 KW. While this represents a typical output power, pulses with power up to 860 KW were recorded.

The position of the laser line was measured in the following way. A portion of the beam was split and fed into a Spex 3/4 meter monochromator. With the wavelength selector set at 5790 A, the laser line was photographed against the background of a known portion of the Hg spectrum. Prior to entering the monochromator, the laser pulse was attenuated by a D=0.4 neutral

density filter and dispersed by ground glass.

While the entrance slit was set at 5μ , no output slit was used.

With knowledge of the reciprocal linear dispersion of the monochromator, we were able to determine the position of the laser line using the 5461.3 \AA emission line of a low pressure Hg lamp as a reference. If a typical laser line, for example, is found to be 0.9 mm to the left (blue) of the 5461.3 \AA Hg line and if the reciprocal linear dispersion of the spectrometer in the wavelength range of interest is 22.199 \AA/mm the lasing wavelength, λ_L , is equal to

$$\begin{aligned}\lambda_L &= 5461.3 \text{ \AA} - 19.98 \text{ \AA} \\ &= 5441.32 \text{ \AA}\end{aligned}$$

The output frequency of the laser can be changed by varying the horizontal vernier on the maximum reflector mount.

With the laser tuned to the desired fundamental frequency of 5441 \AA , the second harmonic crystal can be set up for producing the required UV pump pulse. We initially attempted second harmonic generation with a 90° phase matched temperature tuned ADP crystal. (This required the addition of a $2X$ telescope at the dye laser output to increase the power density of the 5441 \AA radiation and to reduce the beam size to accommodate the ADP crystal.) In 90° phase matching crystals, the fundamental and second harmonic beams propagate normal to the optic axis without birefringence while the wave vector mismatch is made equal to zero by temperature tuning the crystal. The quoted operating temperature for proper phase matching at 2721 \AA is 82°C . The temperature of the crystal was increased to 82°C , at a rate of 1.5°C per minute.

Shortly after the operating temperature was reached, it was observed that the level of the phase matching fluid (freon) surrounding the ADP crystal in the crystal oven had dropped considerably. Attempts to replace the lost fluid

and operate the crystal proved to be futile as fluid loss was still considerable. Even after repairs the unit continued to suffer from loss of freon and in addition, degradation of the ADP crystal faces was observed.

Several attempts by the manufacturer to repair and modify the crystal assembly over the proceeding months, did not produce a satisfactory solution of this problem. After concluding that our difficulties were caused by unavoidable chemical decomposition of the crystal end faces at the operating temperature, we decided to purchase an angle tuned KDP crystal from Cleveland Crystal Co.

The angle-tuned KDP crystal does not require critical alignment to be oriented correctly along the optical axis of the dye laser. It operates at room temperature and requires no reduction of the fundamental beam size. The UV conversion efficiency is high enough that induced fluorescence can be detected visually from a suitable screen placed more than 2 feet from the second harmonic crystal. The output of the dye laser is almost linearly polarized in the horizontal plane and the emerging UV pulse is linearly polarized in the vertical direction.

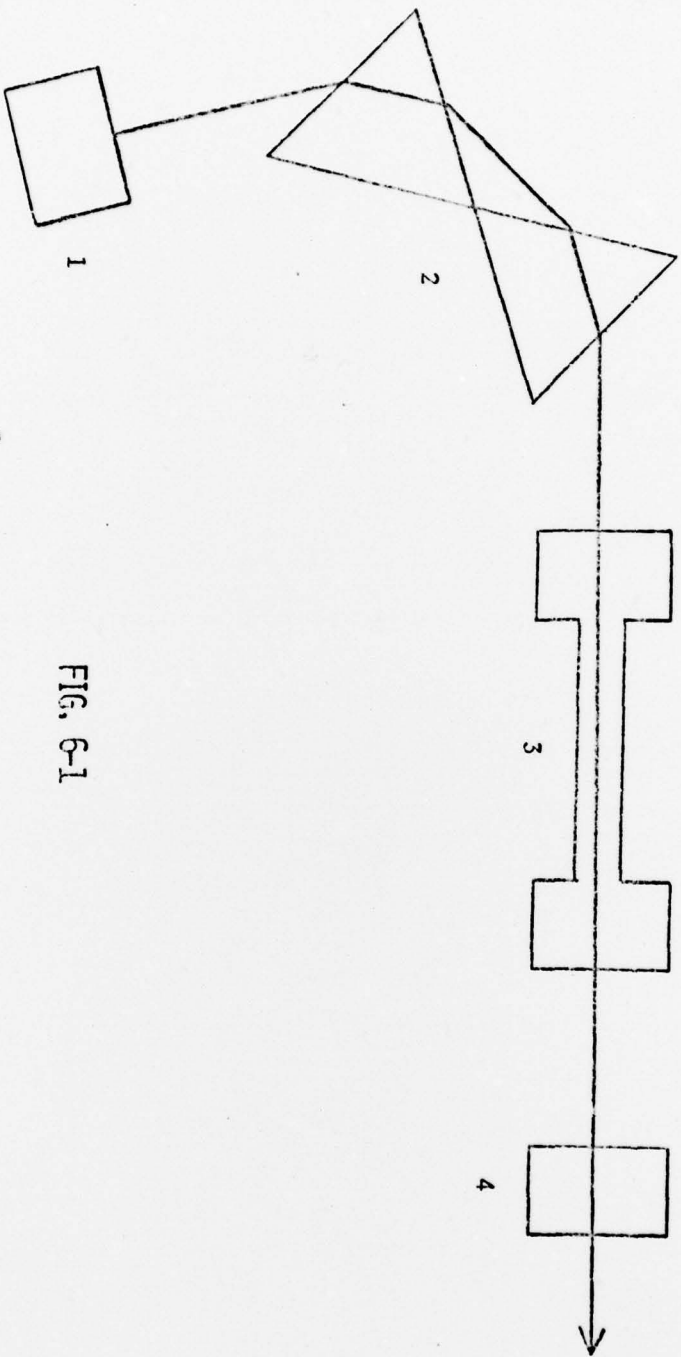


FIG. 6-1

1. MAXIMUM REFLECTOR
2. DP-60 PRISMS (TUNING ELEMENT)
3. FLASHLAMP AND DYE CAVITY
4. OUTPUT REFLECTOR

7. Production of IR laser radiation

Our original plans called for operation of flash lamp Dye laser operating at 9153 \AA^0 and using IR 125 dye dissolved in DMSO as active medium. In assembling and testing the commercial unit which had been purchased for this purpose, we encountered several serious difficulties which we believe ought to be made explicit in this report.

The dye solvent (DMSO) when used in large quantities (about one liter) poses a serious health hazard. The alignment of the laser's optical components is made very difficult by the long path length of the active medium and the nearly total absorption of the He-Ne laser light by the dye. In addition the DMSO freezes in the tubing when the laboratory temperature is less than 18.4°C , while at the same time, the operating efficiency of the dye becomes too low for useful operation at temperature higher than about 20°C .

However, two of the most serious difficulties in the original commercial design of the laser were the very low pumping efficiency of the IR dye by the Xe flash lamp and the rapid degradation of the dye by the high frequency spectral end of the pump radiation. (It should be kept in mind that the IR 125 dye has an absorption peak at 8000 \AA^0).

A second attempt was made using the dye laser cavity to produce a broad band 7000 \AA^0 laser radiation using no tuning elements and Oxazine 720 dye dissolved in Ethanol as the active element with a concentration of $5 \times 10^{-5} \text{ M}$. Under these conditions the power density output of the Oxazine laser was measured to be approximately 550 KW/cm^2 .

The IR 125 solution ($1 \times 10^{-4} \text{ M}$ in DMSO) was placed in a $1 \text{ cm} \times 1 \text{ cm}$ spectrophotometric cell which was positioned inside a cavity consisting of the appropriate reflectors (Fig. (7-1), in a plane parallel configuration. The solution was stirred by a magnetic bar and magnetic stirrer. By hard focusing

the pump pulse inside the limited volume of IR dye we have succeeded in obtaining IR laser emission, but not to such an extent as to allow energy or power measurements. By focusing the IR output on exposed Polaroid film we have barely managed to produce small and faint burn patterns.

A third design employed a special IR cell (Fig.(7-2)) pumped by the Oxazine laser pulse. The dye concentration was optimized at $1 \times 10^{-4} M$ in DMSO and the solution was circulated axially through the active volume. In spite of numerous precautions to minimize losses and to optimise the coupling of the active medium with the pump, the IR laser power was found to be still unsatisfactory. In our opinion the dye efficiency is too low for operation with a pump pulse as long as 600 nsec, which is about the limit for the flash lamp pumped Oxazin laser.

Our fourth design involved the use of a Q-switched Ruby laser as a pump for the IR dye. Preliminary tests were carried out successfully with a passively Q-switched Ruby laser (≈ 40 nsec pulse duration, $\approx 0.4 - 0.5$ Joule pulse energy).

The 6943 \AA^0 radiation was focused by a cylindrical lens into the dye solution using the same geometry shown in Fig.7-2, but after replacing the Max reflector with a high power grating (1200 lines/mm). Reliable IR laser output at the required wavelength (9153 \AA^0) was obtained routinely using an optimum concentration of $1.3 \times 10^{-4} M$ IR 125/DMSO solution. Typical IR pulse energies were measured to be about 10 mJ with pulse durations close to 20nsec. (500 KW power). In our present set up, the passively Q-switched Ruby Laser has been replaced by a new 3.5 J, Pockels Cell Q-switched Holobeam Ruby laser (purchased with Drexel funds).

The IR cell design has also been modified (courtesy of Phase - R Co.). A very satisfactory performance has been obtained using the set up shown in Fig(7-3).

IR pulses in excess of 90-100 mJ (20 nsec duration) can be produced routinely. The output radiation shows good beam quality and moderate divergence. One major advantage of the present set up is that the IR laser beam is wide enough to cover essentially the entire face of the grating. Surprisingly, the intracavity IR laser power is so high that repeated operation has been shown to cause progressive damage of the high power grating used as a tuning element.

The problem can be cured by either lengthening the IR laser cavity (this would also improve the collimation of the laser output) or by replacing the grating with a pair of tuning prisms. This second solution looks less appealing because of the low spectral resolution of the prisms in the wavelength range of interest.

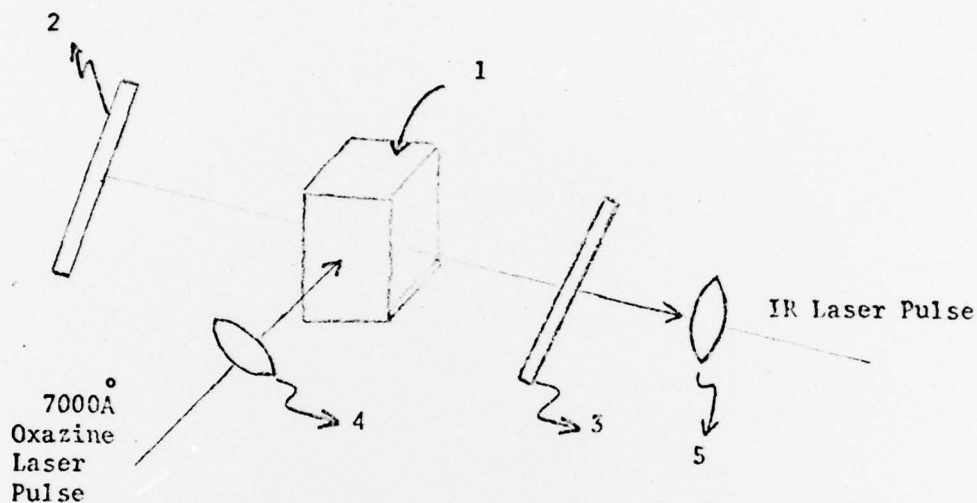


FIG. 7-1

1. 1 CM X 1 CM SQUARE CUVETTE
2. MAX. REFLECTOR
3. OUTPUT REFLECTOR
4. FOCUSING LENS FOR OXAZINE PUMP PULSE
5. FOCUSING LENS TO PRODUCE BURN PATTERNS

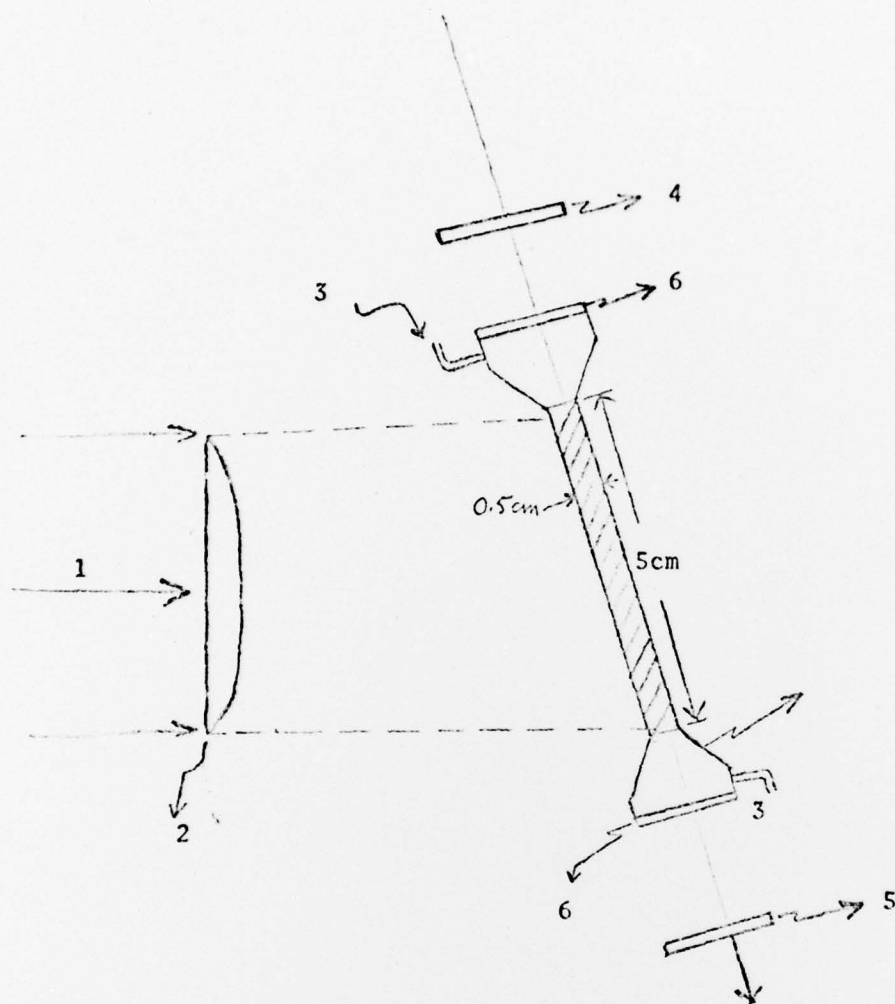


FIG. 7-2

1. 7000Å OXAZINE LASER PUMP
2. CYLINDRICAL LENS
3. CIRCULATING DYE
4. MAX. REFLECTOR
5. IR. OUTPUT REFLECTOR
6. ANTIREFLECTION COATED WINDOW
7. IR DYE CELL

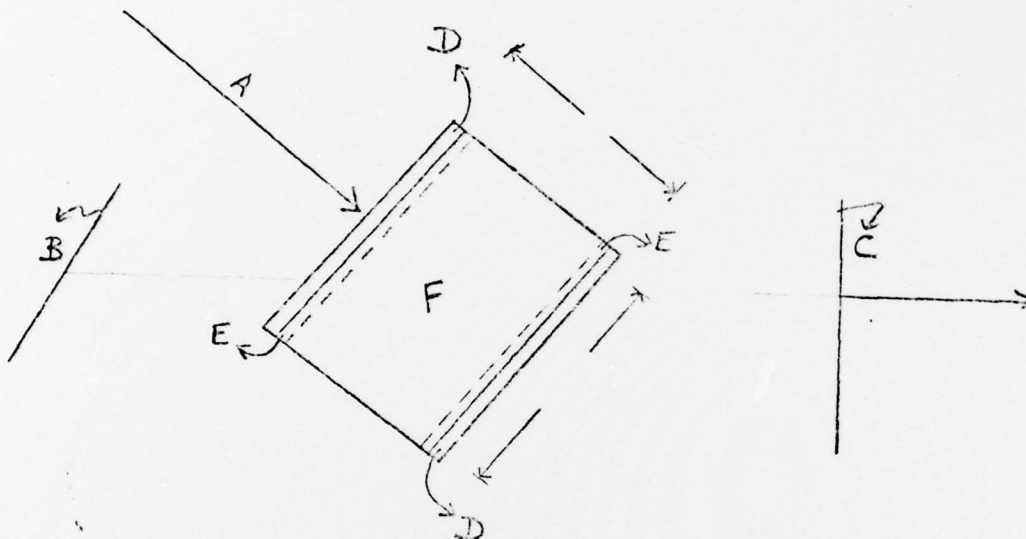


FIG. 7-3

- A 6943 Å PUMP RUBY PULSE (3.5J/20 NSEC)
- B HIGH POWER GRATING (TUNING ELEMENT); 1200 LINES/MM;
BLAZED AT 7500 Å
- C OUTPUT REFLECTOR FOR INFRARED LASER
- D ANTIREFLECTION COATED WINDOW
- E SILICON O-RINGS
- F CIRCULATING DYE; 1×10^{-4} M, IR 125/DMSO

8. Timing Unit

An important requirement in our experimental set up is the ability to control the temporal sequence of the UV pump and of the IR pulse. In the present set up the firing of the Ruby laser can be controlled with good accuracy. A major problem was posed initially by the need to link the Phase-Phase-R Con 540 A⁰ dye laser with the Q-switched Ruby laser.

This was not a negligible difficulty because of the large time jitter of the dye laser spark gap, the slow rise-time of the trigger transformer and the dependence of the corona discharge time on the N₂ pressure in the gap and the air moisture.

To overcome this problem, we have eliminated the Phase-R spark gap and replaced it with a specially selected EG & G spark gap and trigger transformer, characterised by a faster rise time (20 times faster than the original transformer) and a much smaller electronic jitter.

The new unit is sealed, so that it eliminates the need for additional spark gap pressurization. This trigger may have to be replaced more frequently than the original one (it cannot be cleaned inside) but it provides numerous advantages which well compensate for the finite life-time.

The operation of the new tuning unit is illustrated in Fig.(8-1). At $t = 0$ (the onset of the Ruby flashlamp) a pulse enters a master clock to initiate the delay (Fig.(8-2)). The Pockels Cell is triggered by a second pulse from the master clock which is produced after a present time t_1 (in our case 0.68 nsec). A third pulse is finally sent, after a variable delay t_2 , to the modified dye laser triggering unit.

For experiments requiring the input pulse to be the IR pulse one only needs to set $t_1 < t_2$

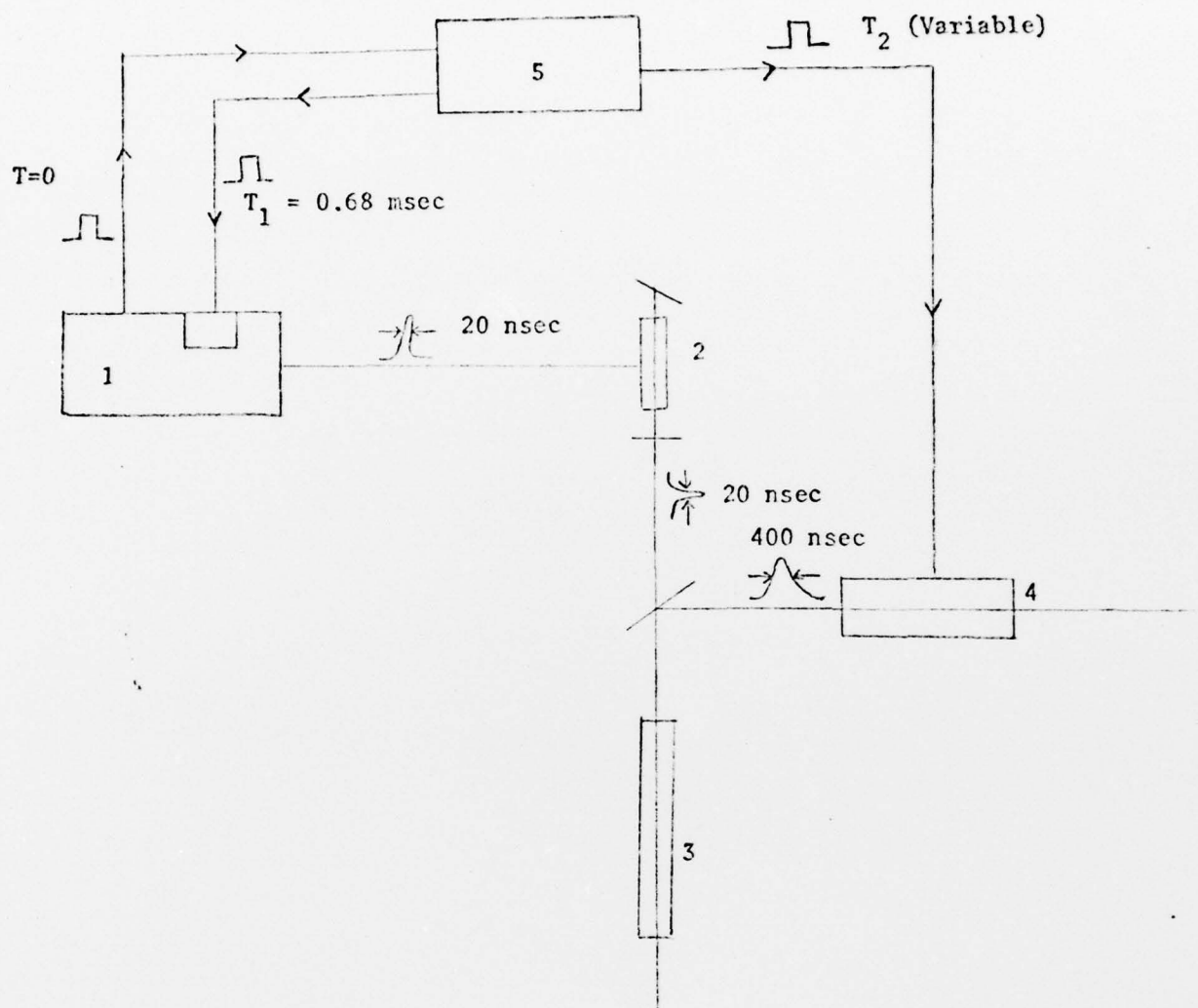


FIG. 8-1

1. RUBY LASER AND POCKELS CELL
2. INFRARED LASER
3. CALCIUM CELL
4. PHASE-R DYE LASER
5. MASTER CLOCK